MASTER THESIS

Memory consolidation and prediction in an in silico neural network

Jordi (J.H.C.) Boons

FACULTY OF SCIENCE & TECHNOLOGY
BIOMEDICAL ENGINEERING
CLINICAL NEUROPHYSIOLOGY

Graduation committee

prof. dr. ir. M.J.A.M. van Putten
prof. dr. R.J.A. van Wezel
dr. ir. J. le Feber
MSc M. Lamberti

15 / 02/ 2022

Samenvatting

Theoretisch werk laat zien dat geheugenconsolidatie (d.w.z. formatie van stabiele geheugensporen) en predictie (d.w.z. anticipatie van toekomstige toestanden) gerelateerd zijn (Hawkins, 2009). Geheugenconsolidatie is onderzocht *in vitro*, waarbij corticale celculturen herhaaldelijk werden gestimuleerd. Er werd bevonden dat corticale culturen niet in staat zijn om geheugen te consolideren bij een hoge cholinergische toon, overeenkomend met in vivo bevindingen. Verder was er geconstateerd dat een hoge cholinergische toon leidt tot een verhoogde neuronale exciteerbaarheid (d.w.z. gemak om een enkel neuron te exciteren) en een verlaagde netwerk exciteerbaarheid (d.w.z. gemak om een netwerk van neuronen te exciteren).
Theoretisch werk laat zien dat het menselijk brein in staat is om voorspellingen te verwerken, wat nodig is om beloning te maximaliseren. Dit proces beschrijft dat neuronen niet alleen informatie kunnen verwerken over het verleden en het heden, maar ook over toekomstige toestanden.
Dit masterverslag bouwt verder op eerder werk, waarin een *in silico* model werd ontwikkeld om onderliggende mechanismes van corticale celculturen te onderzoeken (Le Feber, 2015). Corticale culturen kunnen meerdere geheugensporen consolideren met laagfrequente stimulatie. Het model is niet in staat om een tweede geheugenspoor te consolideren door een te hoge stabiliteit van het netwerk. Ook leidt het toevoegen van acetylcholine enkel tot een verhoogde neuronale exciteerbaarheid. We hebben ervoor gekozen om synaptisch schalen toe te voegen, een vorm van activiteit homeostase. Synaptisch schalen reguleert de vuurfrequentie van neuronen door synaptische sterktes te moduleren.
Het model bestaat uit 100 neuronen, met korte- en lange-termijn synaptische effecten en is uitgebreid met activiteit homeostase. Simulaties met- en zonder acetylcholine zijn uitgevoerd om geheugenconsolidatie met laagfrequente stimulatie te onderzoeken. Predictie is onderzocht met elektrische stimulatie met intervallen tussen stimuli van een bekende distributie.
Resultaten laten zien dat het model is minder stabiel met activiteit homeostase en dat het mogelijk is om een tweede geheugenspoor te induceren. Activiteit homeostase heeft een kritische rol in de reductie van netwerk exciteerbaarheid bij acetylcholine. De toename in vuurfrequentie door acetylcholine leidt tot het afschalen van synaptische sterktes. Deze afname zorgt voor het verspreid vuren van neuronen en bemoeilijkt geheugenconsolidatie.
De analyse van predictie laat zien dat informatie afhankelijk was van de distributie van de stimulus intervallen. Verder vonden we dat stimulusreacties voor de meeste ‘mutual information’ zorgde.
We concludeerde dat activiteit homeostase noodzakelijk is voor geheugenconsolidatie met laagfrequente stimulatie. Dit betekent niet dat dit ook noodzakelijk is *in vitro*, maar dat de stabiliteit van synapsen een belangrijke eigenschap is.
Verder is activiteit homeostase verantwoordelijk voor overgang van een gesynchroniseerd vuurpatroon naar verspreid vuren. Predictie is niet bewezen in dit masterverslag, aangezien de meeste informatie in stimulusreacties zit.

Summary

Theoretical work shows that memory consolidation (i.e. the formation of stable memory traces) and prediction (i.e. the anticipation of future states) are related (Hawkins, 2009). Memory consolidation was investigated *in vitro*, during which cortical cultures were repeatedly stimulated. It was found that cortical cultures are unable to consolidate memory with a high cholinergic tone, resembling *in vivo* findings. Furthermore, a high cholinergic tone increased neuronal excitability (i.e. ease of exciting a single neuron) and decreased network excitability (i.e. ease of exciting a network of neurons).
Theoretical work shows that the human brain is capable of predictive processing, which is necessary to maximize rewards. This describes that neurons can process information not only about the present or past but also future states.
This thesis builds on previous work, in which an *in silico* model was developed to investigate underlying mechanisms of cortical cultures (le Feber, 2015). Cortical cultures can consolidate multiple memory traces with low-frequency stimulation. However, the model can not consolidate a second memory trace due to high network stability. Furthermore, innervation with acetylcholine (ACh) only increased neuronal excitability, while the network excitability remained high. We opted to include synaptic scaling, a form of activity homeostasis, which regulates the firing frequency of neurons by adjusting synaptic strengths to reduce the stability of the network.
The model consists of 100 neurons, with short- and long-term synaptic effects and is expanded with activity homeostasis. Simulations with and without acetylcholine are performed to investigate memory consolidation with low-frequency stimulation. Prediction is assessed with electrical stimulation with inter-stimulus intervals from a known distribution.
Results show that the *in silico* network is less stable with activity homeostasis and that it is possible to induce a second memory trace with low-frequency stimulation. Activity homeostasis has a critical role in the reduction of the network excitability with ACh. The increase in firing rate by ACh causes activity homeostasis to decrease the synaptic strengths that cause dispersed firing and hampers memory consolidation.
The analysis of prediction found that the information that neurons provided was dependent on the distribution of the inter-stimulus intervals. Furthermore, most mutual information was provided by stimulus responses.
We concluded that activity homeostasis is necessary for memory consolidation with low-frequency stimulation. However, this does not imply that this is needed *in vitro*, but that synaptic stability itself is an important property.
Furthermore, activity homeostasis is responsible for the dynamic switch from a burst-dominated network to dispersed firing with ACh in the model. Prediction was not proven in this thesis, as stimulus responses provided the most information about stimuli.

List of abbreviations

ACh	Acetylcholine
AMPA	α-amino-3-hydroxy-5-methyl-4-isoxazolepropionic acid
AUC	Area Under the Curve
BI	Burstiness Index
CCh	Carbachol
ED	Euclidean Distance
GABA	Gamma-aminobutyric acid
ISI	Inter Stimulus Interval
LTP	Long Term Potentiation
MEA	Multi Electrode Array
MI	Mutual Information
PSTH	Post Stimulus Time Histogram
STD	Short Term Depression
STDP	Spike Timing Dependent Plasticity
STP	Short Term Potentiation

List of Figures

1.1 Multi Electrode Array (MEA) with 64 electrodes. The image in the red square displays the full grid of electrodes (black dots) with surrounding neurons (light structures). The yellow square zooms in on three electrodes with a surrounding neuron [1]. 12

2.1 Measurement data (dots) for synaptic potentiation and depression as a function of the relative spiking of a pre-and postsynaptic neuron. Both negative and positive timings have a unique exponential fit that describes the mathematical expression of STDP (black line). This expression is given in Equation 2.7 18
2.2 Visual representation of the different stimulation paradigms that are used in the experiments. For both experiments, there are six hours of unstimulated activity to find a balance in connectivity and activity. For memory consolidation experiments, stimulation is applied for 15 minutes each hour. In prediction experiments, continuous stimulation is used for 20 hours. 22
2.3 Inter Stimulus Interval distributions that have been used in prediction experiments 23

3.1 Overview of the results used for the validation of control simulations. Panel (a) displays the Euclidean Distance of the synaptic matrices from the initialisation of the network. Panel (b) shows the distribution of excitatory synapses for both simulations with- and without activity homeostasis after the network has found a balance in connectivity and activity. In panel c, two raster plots are displayed that show the neural activity of a simulation for five minutes and during a single burst. Panel (d) displays similar raster plots, but for *in vitro* data. 27
3.2 Euclidean distances ED between synaptic matrices for simulations with activity homeostasis (blue) and simulations without activity homeostasis. The figure displays the results of the memory consolidation experiments in which low-frequency stimulation was applied. For the first four hours, a similar pattern is found for both conditions. Each hour the value of ED increases, but the magnitude of change decreases each hour, resulting in a line that flattens over time. In hours 5 - 8 h, a different set of neurons is stimulated. During these hours, a difference is visible between the two conditions. For the simulations with activity homeostasis, the same pattern is found for stimulation with set A. However, without activity homeostasis, ED is small for each hour and a linear increase is visible. For the remaining hours, set A is stimulated again. For both conditions, ED is small for each hour and the pattern does not resemble any pattern in the previous hours. 28
3.3 Mean Firing Rate (MFR) for *in silico* (left) and *in vitro* (right, obtained from [2]) experiments. In both panels, the MFR is given for control experiments and experiments with ACh/CCh. For *in vitro* data, the MFR for experiments with CCh is each hour significant higher than in control experiments. The *in silico* data displays the same difference. 29

3.4 Each raster plot displays five minutes of spontaneous activity with ACh (or CCh *in vitro*), every dot in the plot represent an action potential. Panel (a) corresponds to a simulation with activity homeostasis, panel (b) to *in vitro* data and panel (c) represents a simulation without activity homeostasis. (b) displays that neurons are firing without synchronicity, with an absence of network bursts. The activity of the neurons is heterogeneous as some neurons are more activity than others. Panel (a) displays the same absence of synchronicity for a simulations with activity homeostasis. Some neurons become very active for a certain amount of time (black horizontal lines). In simulations without activity homeostasis (c), the activity pattern displays network bursts and neurons that fire in synchronise. 30
3.5 Bustiness Index (BI) for both *in silico* data (left) and *in vitro* data (right, obtained from [2]). In both panels, the BI is plotted for control experiments and experiments with ACh/CCh. The right panel displays a relatively large value for BI in control experiments with similar values for each hour. Experiments with CCh results in a significantly lower value for BI for each hour.
In silico, the BI for control simulations is also large, with similar values to the *in vitro* data. Also, a significant decrease in BI is found when ACh is included in the simulation. However, the decrease in BI is not as strong as for the *in vitro* data. 31
3.6 Mean Synaptic Weight for both *in silico* data (left) and *in vitro* data (right, obtained from [2]). In both panels, the mean synaptic weight is plotted for control expriments and experiments with ACh/CCh. The *in vitro* data displays a clear difference between both conditions, as the synapses are stronger in control experiments for each hour. The values for control experiments display little fluctuation over time, whereas the values for CCh are experiencing some fluctuation over time. The plot of the simulations (left) display the same difference. The synapses are stronger in control simulations. Unlike, the *in vitro* data, the values for ACh are not fluctuating. 32
3.7 The probability distribution of the magnitude of the STDP update rule for control simulations (left) and simulations with ACh (right). The probability distribution is visualized between the minimum value (0) and maximum value (0.005). For control simulations, a uniform distribution is visible. It implies that each value is as likely to occur as any other value. For ACh, a different distribution is visible. For the values smaller than 0.004 the probability is nearly zero, a small value for an STDP update is implausible. A peak has formed between 0.004 and 0.005. With ACh, synapses are experiencing larger changes by STDP. 33
3.8 Stimulus response curves for control simulations (left) and simulations with acetylcholine (right). The bin count denotes the mean amount of spikes per 5 ms. The red arrow is placed at the moment that a stimulus is applied (latency = 0 ms). In both panels, a rise in bin count is visible when the stimulus is applied. For control simulations, the peak value is larger, but the width of the peak is smaller. The values after the peak in control simulations are similar to values before the stimulus, whereas in simulations with ACh these bin counts are larger. . 34
3.9 The Euclidean Distance ED in memory consolidation experiments is visualized for *in silico* data and *in vitro* data (right, obtained from [2]). In both panels, data is visualized for control experiments and experiments with ACh/CCh. For control experiments *in vitro*, ED increases each hour for hours 1-4 and 5-8. However, the magnitude of change decreases each hour. This behaviour is also present *in silico*. The stimulation of the first electrode for the second time results in a small increase in ED in each hour such that it is not significantly higher than the baseline value for ED. The left panel displays a different behaviour, ED is small for hours 9-12, but it does not increase each hour.
In vitro experiments with CCh, display a small value for ED each hour during the whole experiments, with some fluctuations. The values for ED in the *in silico* experiments are also small, but no fluctuations are visible. 35
3.10 Effect of parameter values for activity homeostasis and ACh on the firing pattern of simulations with acetylcholine. Each row represents variation in a different parameter, where the left column corresponds to a decrease in the value and the right column represents an increase in value. The raster plots show 5 minutes of activity after the network has found a balance in connectivity and activity. 37

3.11 The Euclidean Distance ED of the prediction experiments with respect to the beginning of the stimulation. In the first two hours, ED strongly increases, representing many changes in synapses. After several hours, the value of ED stabilizes and remains the same for the rest of the experiment. 38
3.12 Panel (a) and (b) show the results of the MI analysis for *in silico* and *in vitro* respectively. The used ISI distribution is shown in panel (c). 39
3.13 Each row displays the MI over stimshifts (left) with the corresponding ISI distribution. For every row, a modification has been applied to either the activity of neurons or to the ISI distribution. The first and second rows (a-d) display the same results, but with a different range for the stimshifts. In the third row, all ISI values have been subtracted by 500 ms and in the last row, all bins with stimulus responses are randomly set to 0 or 1. 42

List of Tables

2.1 Initial values for the variables in the simulations. Table adopted from [3]. 20
2.2 Parameter values used in simulations. The Table is adopted from [3]. 21
2.3 Overview of the different model choices for unstimulated simulations. 23
2.4 Overview of different model choices to assess memory consolidation. Low-frequency stimulation denotes stimulation with a frequency of 0.2 Hz. Tetanic stimulation denotes 10 pulses with 100Hz with 4.9 second intervals. 23

Contents

1 Introduction **10**
- 1.1 Memory consolidation . . . 10
  - 1.1.1 Acetylcholine . . . 10
- 1.2 Prediction . . . 11
- 1.3 Cortical cultures . . . 11
  - 1.3.1 Experiments to show memory consolidation . . . 12
  - 1.3.2 Practical limitations . . . 12
- 1.4 Computational model . . . 13
  - 1.4.1 Activity homeostasis . . . 13

2 Methods **15**
- 2.1 Computational model . . . 15
  - 2.1.1 Structure . . . 15
  - 2.1.2 Synapses . . . 16
  - 2.1.3 Simulations . . . 22
- 2.2 Data analysis . . . 24

3 Results **26**
- 3.1 Validation . . . 26
  - 3.1.1 Simulations with activity homeostasis . . . 26
  - 3.1.2 Validation of the effects of acetylcholine . . . 29
  - 3.1.3 Sensitivity analysis . . . 36
  - 3.1.4 Prediction experiments . . . 38
- 3.2 Prediction . . . 39

4 Discussion **43**
- 4.1 Changes to computational the model . . . 43
  - 4.1.1 Activity homeostasis . . . 43
  - 4.1.2 Acetylcholine . . . 44
- 4.2 Memory consolidation . . . 45
- 4.3 Prediction . . . 45
  - 4.3.1 Mutual information . . . 45
- 4.4 Conclusion . . . 46

Chapter 1

Introduction

In mature neural networks, neurons are connected via synapses. During maturation, the network forms these synapses and activity increases. The network finds a balance in the activity of the neurons and the synaptic connectivity after several weeks. Via these synapses, neurons can excite or inhibit each other. Evidence shows that strong synaptic connections induce network bursts (i.e. short periods of synchronous activity) [4]. It is suggested that this synchronous activity enables neural networks to consolidate memory (i.e. formation of stable memories) [2].
Theoretical work shows that prediction (i.e. anticipation of future states) is related to memory consolidation [5]. However, experimental evidence is scarce. Prediction and memory consolidation can be investigated at many levels: from molecular to cognitive levels. In this thesis, we investigate two network phenomena on memory consolidation and prediction in a small-sized computational model.
First, we give background information on memory consolidation and prediction. After which, cortical cell cultures are discussed. Finally, the reasoning for our computational model will be given with the research questions for this thesis.

1.1 Memory consolidation

In vivo, the consolidation of memory is dividable into two sub-processes [6]. Shortly after receiving the external input, memory traces are temporarily stored in the hippocampus which takes minutes to hours [7]. This process is known as synaptic consolidation, during which the cholinergic tone is high. In the second phase, systems consolidation, memories are transferred to the neocortex via a slower process. It is thought that this process is facilitated by the repeated activation of neocortical areas by the hippocampus during slow-wave sleep, during which cholinergic tone is low [8]. Experiments with *in vitro* neural networks found that repeated activation benefits system consolidation [2]. They found that these cortical cultures converged to a (new) stable balance between connectivity and activity after repeated stimulation. However, it is yet unknown which underlying mechanisms affect synaptic connectivity.

1.1.1 Acetylcholine

Acetylcholine (ACh) has long been accorded a critical role in systems consolidation [9, 10]. ACh is a neuromodulator since it is not directly excitatory or inhibitory, but it changes the response of a group of neurons to subsequent stimulation [11]. *In vivo* studies show that a loss of ACh innervation plays a central role in Alzheimer's disease and cholinergic antagonists induce memory dysfunction [10]. ACh has multiple effects that have been observed in *in vivo* studies, neurons are more sensitive to afferent input, there is less feed-forward excitation of neurons, θ-rhythm oscillations (3.5-7.5 Hz) are increased as well as the firing rate of the neurons and the Long-Term Potentiation of synapses is stronger (i.e. persistent strengthening of synapses based on recent patterns of activity) [9].

One of the most striking effects is that **neuronal excitability** (i.e. the ease of exciting a single neuron) goes up with ACh intervention, yet the **network excitability** (i.e. the ease of a network response by a stimulus) goes down [2, 12]. It is suggested that Short Term Depression (i.e. reduction of information transfer at high-frequency presynaptic spikes) or activity homeostasis are possible underlying mechanisms for the change in network excitability [2]. However, no evidence is found yet.

1.2 Prediction

Theoretical work suggests that the human brain is capable of predictive processing, to increase chances of reward [13]. This process describes the ability to not only incorporate information about past or present states but also future states of the body or environment [13].
Prediction was believed to rely on classical conditioning, supervised learning with feedback rewards, similar to supervised learning paradigms that are often used in machine learning [14]. However, Aceituno et al. found that neurons can predict in an unsupervised manner (i.e. without any explicit feedback) [14]. They suggest that synaptic changes due to the relative timing of pre- and postsynaptic firings have a role in prediction. This phenomenon is known as Spike Timing Dependent Plasticity, of which it is known that it has a role in memory consolidation [5]. This relation makes it interesting to investigate these processes simultaneously.

1.3 Cortical cultures

Ideally, memory consolidation and prediction are investigated *in vivo*. However, it is hard to intervene and record many neurons simultaneously. Therefore, cortical cultures are often used as a model of the *in vivo* cortex.
Cortical cultures, which form eventually neural networks, are created by seeding rodent embryonic or early postnatal cortical cells on a multi-electrode array (MEA) (Fig. 1.1). Within several hours there is a beginning in network formation by individual neurons forming axons, dendrites and synaptic connections. After approximately one week, the neurons show spontaneous activity in the form of dispersed firing. Later in the process, network bursts are visible. These bursts last from 100ms to 200ms. In mature cortical cultures, the cell count can be 150,000 with up to 1100 synaptic connections per neuron [15, 16].
The MEA consists of a grid of electrodes. The diameter of one electrode is $30\mu m$, which is approximately the size of neuronal cell bodies in mammalian brains and have a spacing of 200 μm. The MEAs comprise 8 x 8 electrodes. The electrodes can measure extracellular action potentials. Furthermore, the electrodes can locally stimulate networks by inducing potential gradients in the medium surrounding the cells. Work by Le Feber et al. as well as Dias et al. have confirmed that applying external input to cultured neuronal networks can cause network-wide changes and confirmed that MEAs are a suitable platform for studying memory [2, 17].

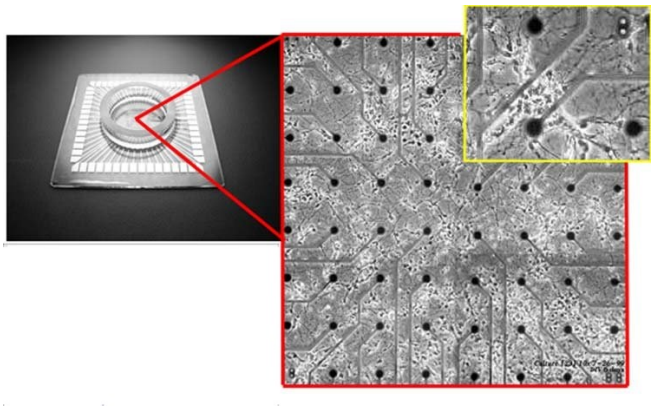

Figure 1.1: Multi Electrode Array (MEA) with 64 electrodes. The image in the red square displays the full grid of electrodes (black dots) with surrounding neurons (light structures). The yellow square zooms in on three electrodes with a surrounding neuron [1].

1.3.1 Experiments to show memory consolidation

In the experiments of Diaz et al., cortical cultures were electrically stimulated. Low-frequency stimulation (0.2 Hz) was applied to a chosen for the first 15 minutes for the first four hours. After this, electrical stimulation was given to a second electrode with the same frequency for the next four hours. Finally, the first electrode was stimulated again with the same paradigm.
They found that stimulation after the first period (15 minutes of stimulation) induced large connectivity changes. However, the magnitude of change decreases for the next 15 minutes. The decrease in the magnitude of change shows that the network converges to a new stable balance between connectivity and activity. Stimulation at the second electrode did induce the same pattern of decreasing connectivity changes over time. When the first electrode was stimulated for the second time, the connectivity changes were small for each stimulation period. It indicates that memory traces remain in the network, even after new stimulations are learned. It indicates that after a second memory trace is induced, the first trace is still present in the network [2].
The experiments were also repeated with cortical cultures that were subjected to treatment with carbachol, an ACh receptor agonist. It is found that these cultures cannot consolidate memory since there was no convergence to a stable state in the stimulation sequence.

1.3.2 Practical limitations

Although MEAs are common in this field of research, there are some practical issues. Even though the size of the electrodes is small and there are a large number of electrodes, the neuron-to-electrode mapping is far from one-to-one [3]. Therefore, it is only possible to record a small number of action potentials in the culture. Furthermore, it is not possible to stimulate an exact number of neurons. Electrical stimulation is applied by one electrode at a time in the experiment.
The biggest flaw is the inability to measure the synaptic strengths of multiple synapses over time, which is relevant for assessing memory consolidation. Only functional connections can be assessed via statistical terms [12]. Using computer simulations, we can measure and change each parameter that is in the model.

1.4 Computational model

The theses of van Veenendaal and Dijkstra showed that important properties of a cortical culture (i.e. bursting and adaptation to stimuli) can be reproduced by a small-scale computational model [18, 3]. This model included single-compartment neurons and multiple synaptic mechanisms, like STDP (i.e. adjustment of synaptic strengths based on the relative timing of pre-and postsynaptic spikes) and Short Term Depression (STD) (i.e. reduction of information transfer at high-frequency presynaptic spikes).
There are several advantages of a computational model compared to *in vitro* experiments. One of the advantages is that the simulations are faster. The exact speed depends on multiple factors, like the size and detail of the model. But proceedings, like harvesting cells from rodents or maturation of the network, do not have to be performed. Furthermore, the degree of controllability is better since we can control and store each desired variable. It is also possible to recall an earlier state of the model, whereas that is not possible with cortical cultures. Unlike in *in vitro*, we can control the number of neurons that are stimulated and we can assess if they are stimulated. Last, the issue of accessibility of synaptic weights is a problem considering memory consolidation analysis. The stability of synaptic weights over time indicate a stable network and with the cortical cultures, it is only possible to measure the weights indirectly. With the model, we know the development of each synapse over time, where the sampling rate is controllable. Furthermore, we have complete control over the mechanisms that are included, whereas *in vitro*, this controllability is much lower.
There are also downsides to a computational model. First, not every mechanism or physiological effect in cortical cultures can be included in the model. Second, mechanisms like STDP and STD are described via mathematical equations and will not be the same as in *in vitro*. The model can be regarded as a suggestive model for mechanisms that may take place in a cortical culture as well as the data analysis techniques that are used to quantify them.
Furthermore, in the existing model, mechanisms of action of ACh are not incorporated, and therefore the model cannot reproduce experimental findings under a high cholinergic tone. In the existing model, the neuronal excitability increases, but there is no dispersed firing.

1.4.1 Activity homeostasis

In the thesis by van Veenendaal, it was found that with additive STDP, a synaptic-weight-independent STDP description, it is possible to consolidate memory when tetanic stimulation is used (i.e. ten high-frequency stimuli that occur every 5 seconds) [18]. However, it was impossible to accomplish this with low-frequency stimulation (i.e. a single pulse every 5 seconds). It was suggested that this is due to the high stability of the networks caused by the additive STDP. Work by Billings & van Rossum, found evidence for this suggestion [19]. With additive STDP, strong synapses are likely to become even stronger where the same logic follows for weak synapses [19]. It is therefore hard to induce changes in the network.
It was possible to consolidate memory with low-frequency stimulation in the experiments of Dias et al. in cortical networks [2]. That means that something is missing in the current model. Therefore, it is opted to include a biologically plausible mechanism that reduces stability in synaptic strengths to accomplish memory consolidation with low-frequency stimulation.
It is opted to add activity homeostasis to the model since this is a well-studied mechanism [20, 21]. This mechanism regulates the firing rate of neurons. Different regulatory biological processes, that control the number of synapses, network excitation and intrinsic excitability, are contributing to activity homeostasis. This thesis focuses on synaptic scaling. Evidence describes that changes in synaptic strength over a long timescale are accompanied by activity homeostasis to prevent neurons from being silent or hyperactive [20]. Turrigiano found that this activity homeostasis mechanism is present *in vivo* as well as *in vitro* [20]. It is suggested that neurons can detect their firings through calcium-dependent sensors [21]. Furthermore, it is believed that synaptic scaling requires network-wide changes in activity by the release of factors by many neurons [22]. *In vivo*, there is not only one synaptic scaling mechanism. Nested homeostatic mechanisms operate over different temporal and spatial scales to regulate network activity [21]. The complexity of these nested mechanisms will be reduced by only looking at one network-wide synaptic scaling mechanism.

Research questions

The findings in the previous theses of Dijkstra and van Veenendaal, and the results from the *in vitro* study of Dias et al. lead to the research questions of this thesis [2, 3, 18].
We hypothesize that the addition of the activity homeostasis mechanism will enable learning and consolidate multiple memory traces in computational cortical culture with low-frequency stimulation. We believe that the increase in neural excitability will cause a decrease in feed-forward excitation of neurons, dispersed firing and the inability to consolidate memory.
The goal of this thesis is to validate this hypothesis. Therefore, the experiments performed by Dias et al. are repeated with our computational neuronal network. We will test whether it is possible to reproduce the findings of Dias et al. and assess the mechanisms that are causing these results. Furthermore, simulations with stimulation with inter-stimulus intervals from a known distribution will be performed to investigate prediction. Simulations will be performed that will answer the following research questions:

1. What is the effect of including activity homeostasis to the existing computational model on the induction of a second memory trace?

2. Which underlying mechanism(s) cause the change from a burst dominated network to dispersed firing when the action mechanisms of Acetylcholine are included in a computational model?

3. Which underlying mechanisms cause the inability to consolidate memory when acetylcholine is introduced in a computational neural network?

4. Is a computational model of a cortical culture able to predict the occurrence of stimulations?

Chapter 2

Methods

2.1 Computational model

In modelling, it is the art to develop a model with a minimum level of detail that can produce the desired functionality to answer the research questions. Unnecessary phenomena might conceal the origin of observed behaviour. The work in this thesis builds on an earlier developed model [3, 18], and aims to include responses to low-frequency stimulation under low and high cholinergic tones that were recently got in [2].

2.1.1 Structure

In line with previous work, we use a small-sized network of 100 cortical neurons in our model [3, 18]. 80 % of the neurons are excitatory, in agreement with biological data [23]. In contrast to our small-sized network, a cortical culture can consist of $\sim$ 150,000 neurons. Every neuron can have up to $\sim$ 1100 synapses, which account for a density of $<$ 1 % [24].
Each neuron is connected to approximately 50 % of the other neurons, which accounts for a synaptic density of 0.5, to compensate for the small size of the network. Synaptic efficiency is increased as a compensation mechanism. Axons are modelled as delays since these are not included in the neuron model, which defines the time difference between a pre-and post-synaptic spike, in line with Dijkstra [3]. The delays are taken from a uniform distribution of [1, 25] ms.

The neuron

A set of differential equations describe the dynamics of each neuron in the model. We opted to use the Izhikevich descriptions for the neural cell dynamics since they can produce biologically relevant dynamics with efficient computation, in contrast to the computational costly Hodgkin-Huxley equations [25]. The Izhikevich equations describe the membrane potential v and the recovery variable u, that accounts for slow ion currents, which are visualized below in equations 2.1 and 2.2. This neuron model does not include axons or dendrites since it is a single compartment neuron [25].

$$\frac{dv_i}{dt} = 0.04v_i^2 + 5v_i + 140 - u_i + I \tag{2.1}$$

$$\frac{du_i}{dt} = a_i(b_i v_i - u_i) \tag{2.2}$$

I represents the input current of the neuron and parameters a, b, c, d define the type of the cortical neuron. If the membrane potential v reaches $30mV$, the neuron fires and the variables v and u are reset according to equation 2.3.

$$\text{if } v_i \geq 30mV, \text{ then } \begin{cases} v_i \leftarrow c_i \\ u_i \leftarrow u_i + d_i \end{cases} \tag{2.3}$$

In accordance with Izhikevich, we introduce heterogenecity by assigning each neuron its own unique set of parameters and therefore unique dynamics [25]. The parameters of excitatory neurons (see Table 2.2) are chosen from a uniform distribution between the parameters of *regular spiking* (RS) and *chattering* (CH) neurons, with a bias towards RS neurons [25]. For each neuron, a random variable r is chosen from the uniform distribution $U(0,1)$ and squared to bias it towards zero. The parameters a,b,c,d are then calculated as $a = (1-r)\cdot a_{RS} + r \cdot a_{CH}, b = 1 - r \cdot b_{RS} + r \cdot b_{CH}$ etc. $r = 0$ corresponds to a RS neuron, whereas $r = 1$ corresponds to a CH neuron. The same approach is used for the parameters of the inhibitory *fast spiking* (FS) and *low threshold spiking* (LTS) neurons. However, there is no bias introduced.
The forward Euler method is chosen as solver for the differential equations. The membrane potential is updated twice as fast since it changes relatively fast compared to the reco variable u [3]. The update sequence with the Euler forward method looks like:

for all neurons n **do**

$$v_{n,t+0.5} = v_{n,t} + 0.5 \cdot dt \cdot (0.04v_{n,t}^2 + 5v_{n,t} + 140 - u_{n,t} + I_n)$$
$$u_{n,t+1} = u_{n,t} + dt \cdot a_n \cdot (b_n \cdot v_{n,t+0.5} - u_{n,t})$$
$$v_{n,t+1} = v_{n,t+0.5} + 0.5 \cdot dt \cdot (0.04v_{n,t+0.5}^2 + 5v_{n,t+0.5} + 140 - u_{n,t+1} + I_n)$$

Stimulation

With the computer model, we can give stimulations with high precision. In the model, a neuron is stimulated by setting its membrane potential v to $30mV$, such that a spike is detected at the next update. In the previous model by Dijkstra, it was only possible to stimulate with repetitive Inter Stimulus Intervals (ISIs). In the current model, it is possible to read ISIs from a file such non-repetitive stimulations can be given, like in the prediction experiment.

2.1.2 Synapses

Synapses, either chemical or electrical, connect outgoing axons with the dendrites of a target neuron. In the model, solely chemical synapses are included since they are most common in cortical networks. Excitatory synapses cause depolarization to facilitate excitability (action potentials), whereas inhibitory synapses induce hyperpolarization to inhibit excitability. Neurons whose axons connect to excitatory terminals are defined as excitatory neurons and the same logic follows for inhibitory neurons.
The synaptic efficacy can change on both short and long timescales. It is necessary to include long-term plastic effects since these are necessary for learning and consolidation [26]. However, short-term effects should not be excluded since most long-term changes take place in network bursts, which are strongly affected by short-term changes.
The short term effects that are included in this model are Short Term Depression (STD) (i.e. weakening of synapses due to depletion of neurotransmitters) and Short Term Potentiation (STP) (i.e. strengthening of the synapse after multiple activations in short succession). The model of Makram et al. includes both STP and STD by describing the fraction of available neurotransmitter that is released by the n^{th} spike y_n and the relative amount of neurotransmitter after the n^{th} spike R_n, for which the equations are given in 2.4 and 2.5 respectively. The value of y_n increases as pre-synaptic spikes arrive at a synapse and decays to the initial value U. R decreases at each pre-synaptic action potential and increases over time back to one.

$$y_{n+1} = y_n \cdot exp(\frac{-\Delta t}{\tau_{facil}}) + U \cdot (1 - y_n \cdot exp(\frac{-\Delta t}{\tau_{facil}})) \tag{2.4}$$

$$R_{n+1} = R_n \cdot (1 - y_{n+1}) \cdot exp(\frac{-\Delta t}{\tau_{rec}}) + 1 - exp(\frac{-\Delta t}{\tau_{facil}}) \tag{2.5}$$

τ_{facil} and τ_{rec} are the time constants for facilitation and recovery respectively and Δt denotes the time since the previous spike.

Neurotransmitters activate selective ion channels at post-synaptic terminals, which will change conductivity to that ion. This conductivity change follows a certain profile, that resembles the difference between two exponentials that describe the increase and decrease of conductivity to that certain ion. However, in common with Dijkstra, we assume that the arrival of a presynaptic action potential leads to an instant increase in conductivity proportional to the amount of released neurotransmitter [3]. The conductivity shows an exponential decay with a time constant of τ_{syn}, which is defined by the type of neurotransmitter. We will assume that all synapses are AMPA and $GABA_A$ which have time constants of 5.26 ms and 5.6 ms [27]. However, for simplicity 5 ms is used.

Post-synaptic current

In cortical cultures, changes in conductivity causes a current flow into or out of the dendrites. For simplicity, we ignore the dependency of this current on the potential difference across the cell membrane since these fluctuations are rather small (except during action potentials) and we describe the post-synaptic current by:

$$\frac{dI_{syn}(t)}{dt} = -\frac{I_{syn}(t)}{\tau_{syn}} + A \cdot S(t) \cdot y_n \cdot R_n \cdot \delta(t - t_n) \tag{2.6}$$

The first term describes the exponential decay of the current, the second term accounts for the instantaneous increases of the current due to action potentials arriving at $t = t_n$. This current is linearly proportional to the amount of released neurotransmitter ($y_n \cdot R_n$). A is a constant scaling factor that is determined by the type of synapse (for example Excitatory-Excitatory). $S(t)$ described the relative strength of synapses over time. For excitatory synapses, this is bounded to [0, 1], whereas inhibitory synapses are in the range of [-1, 0]. We described S over time since it is affected by long-term effects that will be discussed later. $S(t)$, y_n and R_n are bound at $abs(1)$. Therefore, the scaling factor A describes the maximum current that can persist in the dendrite.
In cortical cultures, dendrites sum and filter incoming currents arriving at the post-synaptic terminal. However, in the model dendrites are not explicitly included. The input to a neuron is defined as the sum of momentary currents of the synapses that are connected to this neuron.

Spike Timing Dependent Plasticity

For one of our long-term plasticity mechanisms, we use spike-timing-dependent plasticity (STDP), which cause both potentiation and depression of synapses [28]. Many STDP models exist (as listed in [19]), but they have in common that they describe the change in synaptic strength to the timing between pre-and postsynaptic neurons. In Figure 2.1, experimental evidence is given for this phenomena. If a postsynaptic neuron fires after a presynaptic neuron, then the synaptic strength increases and vice versa. In this thesis, we use an additive STDP model and a multiplicative STDP model, for which the equations can be generalized by equation 2.7. In this equation, the change synaptic strength S is described as a function of factor F_+ or F_-, the time-difference between spikes Δt and a time-constant τ_{STDP}.

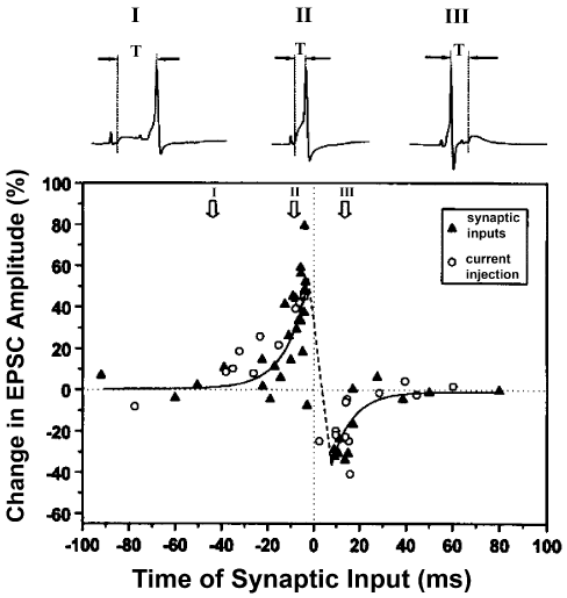

Figure 2.1: Measurement data (dots) for synaptic potentiation and depression as a function of the relative spiking of a pre-and postsynaptic neuron. Both negative and positive timings have a unique exponential fit that describes the mathematical expression of STDP (black line). This expression is given in Equation 2.7

$$\Delta S = \begin{cases} F_-(S) \cdot exp(\frac{-\Delta t_{STDP}}{\tau_{STDP}}) & if\ t_{pre} > t_{post} \\ \\ F_+(S) \cdot exp(\frac{-\Delta t_{STDP}}{\tau_{STDP}}) & if\ t_{pre} < t_{post} \end{cases} \tag{2.7}$$

In the additive model, the weight change is not dependent on the synaptic weight. Thus we write for the additive factors $F_+ = A_+$ and $F_- = -A_+ \cdot 1.05$. The initial value can be found in table 2.1. A_-/A_+ can be regarded as the learning rates. The magnitude of depression is larger than for potentiation. This is necessary for achieving a stable state of the neural network. The additive model tends to form a bimodal distribution since strong synapses are likely to become even stronger and weak synapses tend to weaken [19]. However, experimental data of synaptic changes due to paired spikes have shown that synaptic depression is multiplicative. Data for potentiation is less clear, so for the multiplicative model we define the following factors $F_+ = A_+$ and $F_- = 2 \cdot S \cdot A_-$ [3]. A factor of 2 is added to induce a uniform distribution that is centred around 0.5.

In the work of van Veenendaal, it was found that memory consolidation is not possible with multiplicative STDP due to instability [18], whereas it is possible in some cases with additive STDP. However, it is unknown how the model will behave with the addition of the activity homeostasis. Therefore, both options will be investigated. Since the goal of modelling is to show the desired phenomena, we will choose the model that can reproduce consolidation experiments that have been performed *in vitro*. Although the synaptic distribution of the multiplicative STDP model seems biologically plausible, this is not of our interest and will not be an important factor.

Another consideration for the STDP model is the spike pairing scheme. In the case of an all-to-all scheme, all the spike pairs within the STDP window contribute to weight changes. In line with Dijkstra, we opt for a reduced symmetric scheme. With this scheme, only a small part of the spike pairs contribute to weight changes.

Unlike STDP for excitatory synapses, the rules for inhibitory synapses are less clear. Inhibitory neurons should increase in strength after the post-synaptic neuron has not fired. But it is impossible to give the timing of this non-existing event. Therefore, it is assumed that the strength of all inhibitory synapses is -0.5 thus, the inhibitory synapses have no long-term plasticity.

Activity homeostasis

In vitro and *in vivo*, activity homeostasis prevents both hyperactivity and falling silent of neurons by adjusting synaptic strengths [20]. The description of the activity homeostasis should therefore describe the change in synaptic weight based on previous activity. The chosen description can be found in the equation below and is based on the work of Toyoizumi [29].

$$\frac{dS}{dt} = S(t) \cdot \frac{1}{\tau_{HS}} \cdot (y - \hat{y}) \tag{2.8}$$

The change in synaptic weight S over time is described by the value of S on time t, a time-constant τ_{HS}, the mean activity of the network and a threshold $\hat{y}$. The mean activity is calculated by taking the mean of all action potentials over the last eight hours and dividing by the number of recorded neurons. A value of eight hours is chosen since activity homeostasis has a timescale from hours to days and this value gave a stable solution in simulations [20]. The values used in the simulations can be found in Table 2.2. It can be derived that when activity $y > \hat{y}$, the synaptic strength will decrease and vice versa. This is in line with the action mechanism that is found *in vitro* and *in vitro* [20]. However, the description in the model only applies to excitatory neurons and synapses, whereas *in vitro* and *in silico* also inhibitory systems are influenced by activity homeostasis [20]. However, to maintain the simplicity of the model, this system was not included.

Acetylcholine

One of the action mechanisms of acetylcholine (ACh) is that it induces biphasic changes in the activity of pyramidal neurons (i.e. excitatory population), consisting of fast inhibition followed by a slow depolarization [9]. The fast inhibition is mediated by an increase in the excitability of interneurons (i.e. inhibitory population), which causes an increase in their firing rate. The slow depolarization is mediated through Muscarin M1 receptors by the closure of slow potassium channels in pyramidal channels to increase their resting membrane potential and to reduce hyperpolarization after an action potential.
In the model, the fast inhibition will be ignored to reduce the complexity of the model. We can ignore it since it is a short-lasting effect. The decreased depolarization is modelled by a decrease in parameter d of the Izhikevich neuron. This parameter accounts for the slow potassium and sodium channels after a spike reset, which causes hyperpolarization of the membrane potential [25, 30]. For simulations with ACh, we describe parameter d_{ACh} as, $d_{ACh} = d \cdot n$, where n is bound by [0, 1] and the d is the normal value for the RS and CH neurons. Parameter n is the same for each neuron, so no distinguishing is made between RS and CH neurons.
Furthermore, ACh decreases the probability of GABA release onto perisynaptic compartments of pyramidal neurons. It is therefore less likely that excitatory neurons are inhibited, thus there is a reduction in postsynaptic inhibition [30]. This increases the excitability of the pyramidal neurons.
In the model, it is opted to model the decrease in GABA release by decreasing the absolute strength of Inhibitory-to-Excitatory synapses, A_{IE}. By reducing the strength of these synapses, it is less likely that the inhibitory neurons can inhibit the excitatory population. Therefore, the result is, like *in vivo*, that there is a decrease in postsynaptic inhibition of excitatory neurons.
For the absolute strength of each IE synapses $A_{ACh,IE}$ in simulations with acetylcholine, we write $A_{ACh,IE} = A_{IE} \cdot m$, where m is bound by [0,1]. Thus creating a uniform decrease in all IE synapses.

Intrinsic activity

Without stimulation, there is no external input to the network. However, the network should show spontaneous activity, as seen in cultured cortical neurons. Therefore, we should add some kind of intrinsic activity. Different methods exist for this, like pacemaker cells and synaptic noise injection. Pacemaker cells fire at a regular rate and induce network responses. With noise injection, the noise causes spontaneous spiking of neurons, making them intrinsically active. The main difference is that pacemaker cells make up a small part of the network, whereas with noise injection each neuron will be potentially intrinsically active. In the work of Dijkstra, satisfying results were achieved with Gaussian synaptic noise injection and there was no reason to derive from this approach [3]. With noise injection, the membrane potential v of the neurons are updated using the Euler-Maruyama method.

Parameter choices and initial values

The initial values for the simulations are summarized in table 2.1. In table 2.2, the values of parameters and their origin are summarized.

Table 2.1: Initial values for the variables in the simulations. Table adopted from [3].

	Parameter	Sym.	Init. value(s)		Origin
Neuron					
	Membrane potential	v	-65		[25]
	Reco variable	u	$-65 \cdot b$		[25]
Synapses			*Excitatory*	*Inhibitory*	
	Synaptic strength	S	$U(0,1)$	-0.5	[3]
	Used neurotransmitter	y	U	U	[31]
	Available neurotransmitter	R	1	1	[31]

Table 2.2: Parameter values used in simulations. The Table is adopted from [3].

	Parameter	Sym.	Init. value(s)				Origin
Structure							
	Number of neurons	N	100				[3]
	Number of exc. neurons	N_e	80				[3]
	Number of inh. neurons	N_i	20				[3]
	Connection density	$-$	50 %				[3]
	Axonal delays	$-$	U(1,25)				[3]
Neuron			*Excitatory*		*Inhibitory*		
	Auxillary variable	r	U(0,1)		U(0,1)		[25]
	Reco speed of u	a	0.02		0.1 - 0.08 $\cdot$ r		[25]
	Sensitivity of u to v	b	0.2		0.25 + 0.05 $\cdot$ r		[25]
	Reco speed of u	a	0.02		0.1 - 0.08 $\cdot$ r		[25]
	Reset value of v	c	-65+15 $\cdot r^2$		-65		[25]
	Reset value of v with ACh	c	-53+15 $\cdot r^2$		-65		
	Reset value of d	d	8 - 6 $\cdot r^2$		2		[25]
	Reset value of d with ACh	d	0		2		
Synapses			EE	IE	EI	II	
	Reco value of y	U	0.59	0.049	0.16	0.25	[32, 33, 34]
	Max. efficiacy [VS^{-1}]	A	10.8	32.5	43.2	43.2	[18, 35]
	Facil. const. [ms]	τ_{facil}	0	1797	376	21	[32, 33, 34]
	Reco const. [ms]	τ_{rec}	813	399	45	706	[32, 33, 34]
	Synaptic const. [ms]	τ_{syn}	5	5	5	5	[27]
STDP							
	Potentiation rate	A_+	0.005				[28]
	Depression rate	A_-	$A_+ \cdot 1.05 \cdot 2$ or A_+				[28]
	Time constant [ms]	τ_{STDP}	20				[28]
Activity homeostasis							
	Time constant [h]	τ_{HS}	8				
	Target firing rate	$\hat{y}$	0.44				[2]
Noise							
	On exc. neurons	σ	2.2				[3]
	On inh. neurons	σ	0.88				[3]

Sensitivity analysis

The chosen values for the parameters, of the activity homeostasis and acetylcholine are empirically determined. We altered each parameter -10% and +10% of its chosen value to determine the sensitivity of the chosen values. For parameter d of the Izhikevich neuron, we only increase the value by 10%, as the chosen value is at the minimum of the range. Our outcome measure is the dispersed firing, as this is considered the most striking outcome for the validation of acetylcholine.

2.1.3 Simulations

Stimulated

Two unique experiments will be executed with stimulated networks: memory consolidation- and prediction experiments. They have in common that the model develops during 6 hours without stimulation and that a set of nine neurons (seven exc. and two inh. neurons) are stimulated simultaneously, following van Veenendaal [18].
In the memory consolidation experiment, a set of nine neurons (set A) is stimulated during four periods of fifteen minutes, with 45-minute intervals, see Figure 2.2A. The same paradigm is repeated for a unique set of neurons (set B) during hours 5-8. After this period, set A is stimulated again for hours 9-12. This experimental design resembles the design of Dias et al. [2]. However, we stimulated a set of neurons whereas Dias stimulated an electrode. For each combination of the parameters in table 2.4, five realizations were performed for 18 hours in total for this experiment.
From the results of the simulations of Table 2.4, it was conducted that the combination additive STDP, activity homeostasis and low-frequency stimulation gave the results that resemble the *in vitro* results best, so for further experiments these settings were used.
To validate the effect of acetylcholine on memory consolidation, we performed five realisations with settings for acetylcholine (see Table 2.2).
Five realisations have been performed with normal settings and five realisations with the settings for acetylcholine.
In prediction experiments, only one set of neurons is stimulated for twenty hours.

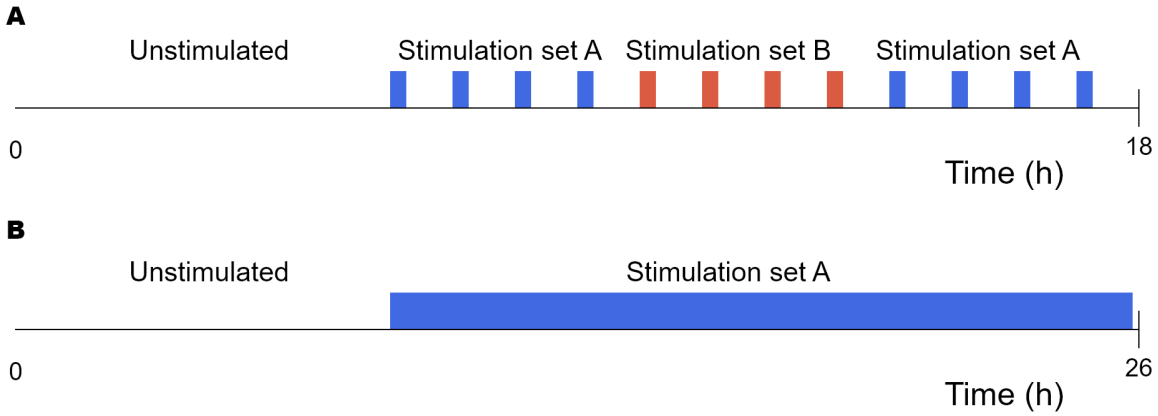

Figure 2.2: Visual representation of the different stimulation paradigms that are used in the experiments. For both experiments, there are six hours of unstimulated activity to find a balance in connectivity and activity. For memory consolidation experiments, stimulation is applied for 15 minutes each hour. In prediction experiments, continuous stimulation is used for 20 hours.

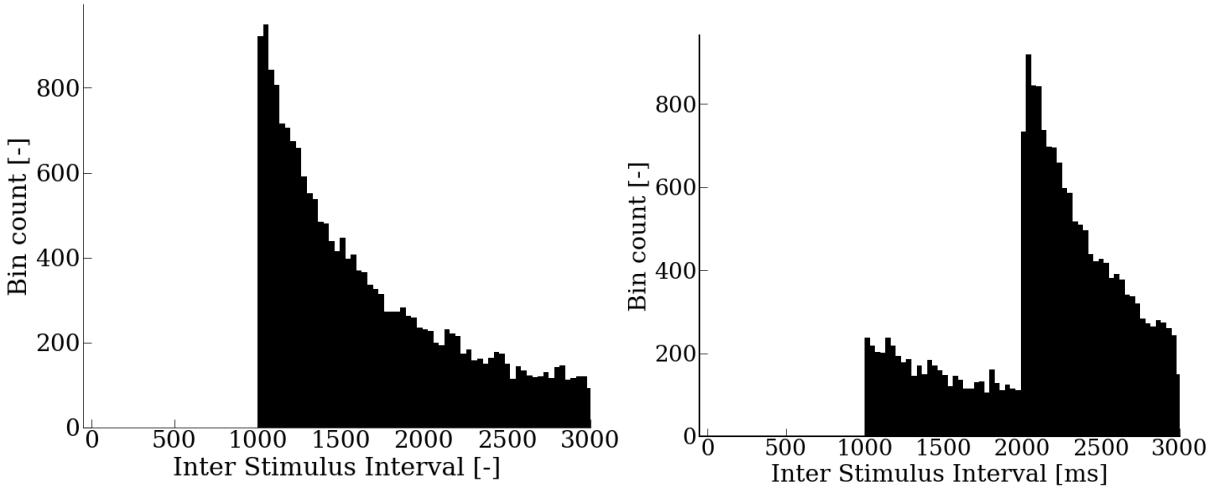

((a)) Histogram of the inter-stimulus interval distribution used for validation with *in vitro* data. The distribution displays that the minimum inter-stimulus interval is 1000 ms. This is also the most probable inter-stimulus interval, as the bin count is the highest. For larger intervals, the probability decreases.

((b)) Histogram of the inter-stimulation interval distribution after modifications have been made. All inter-stimulus intervals in the range of (1000,2000) ms are increases by 1000 ms. The intervals in the range of (2000, 3000) are reduced by 1000 ms. The minimum interval is still 1000 ms. However, it is not the most probable interval anymore. An interval of 2000 ms is the most likely to occur. For larger intervals, the probability decreases.

Figure 2.3: Inter Stimulus Interval distributions that have been used in prediction experiments

Unstimulated

Realizations without stimulations have been performed to assess the difference in network dynamics between normal settings and networks treated with ACh without an influence by stimuli. In each realisation, the network develops for six hours. We will then perform any analysis with the data starting at $t = 6h$ until the end of the realisation, which is 26 hours. We chose this value since the memory consolidation experiments (18h) and prediction experiments (26h) are of this length. In this way, the unstimulated realisations serve as a baseline for the experiments.

Table 2.3: Overview of the different model choices for unstimulated simulations.

Description	Activity homeostasis	Acetylcholine
Normal settings	Yes	No
No activity homeostasis	No	Yes
Acetylcholine	Yes	Yes

Table 2.4: Overview of different model choices to assess memory consolidation. Low-frequency stimulation denotes stimulation with a frequency of 0.2 Hz. Tetanic stimulation denotes 10 pulses with 100Hz with 4.9 second intervals.

STDP update rule	Activity homeostasis	Stimulation
Additive	With	Low-frequency
Multiplicative	Without	Tetanic

2.2 Data analysis

Burstiness

The method that is used to quantify burstiness, is taken from Wagenaar et al. [36]. With this method, it is unnecessary to identify individual bursts. Recorded action potentials are divided into five-minute segments. In every segment, the spikes are sorted into 300 1-second-long bins. The fraction of the total number of spikes accounted by 15 % of the bins with the largest counts (f_{15}) is determined. The burstiness index (BI) is then calculated by $BI = (f_{15} - 0.15)/0.85$ and bounded by [0, 1]. If $BI \sim= 1$, then all spikes occur in bursts. For $BI \sim= 0$, there is a complete absence of bursts.

Euclidean distance between weight matrices

The Euclidean Distance (ED) quantifies the magnitude of change between two equally sized vectors or matrices. In this analysis, we use it to get information about the magnitude of change of the network by calculating the ED of the synaptic weight matrices. In the equation $w_{ij}(t)$ denotes the synaptic weight of the synapse from neuron i to j at time t. t_0 is the reference point in time for the calculation of ED.

$$ED(t) = \sqrt{\sum_{i=1}^{n}\sum_{j=1}^{n}(w_{ij}(t) - w_{ij}(t_0))^2} \tag{2.9}$$

Post-stimulus time histograms

To assess the effectiveness of stimulation, we computed Post-stimulus time histograms (PSTH) per stimulation period for all stimuli. The PSTH shows the summed number of action potentials per 5ms bins during the interval of 300ms before until 300ms after the stimulus. The area under the curve (AUC) between 5ms and 300ms latency was computed per stimulation period. We subtract the AUC from -300ms - 0ms from the computed value, to account for the differences in mean firing rate between control and ACh simulations.

Validation of the effects of acetylcholine

In vivo, the following effects of acetylcholine have been observed: an increase in firing rate decreased synchronicity, decreased feed-forward excitation, increased long-term potentiation and decreased memory consolidation [9]. We analyzed the increase in firing rate by computing the difference in mean firing rate in simulations with acetylcholine and control simulations. The mean firing rate is computed for each hour by summing all action potentials and dividing by the number of recorded neurons and time.
The decreased synchronicity will be assessed in a visual and quantified manner. For the visual analysis, we make scatterplots of action potentials for each recorded neuron over time, also known as raster plots in neuronal research. Via this method, we can observe whether network bursts occur. We will also use the burstiness index to quantify the burstiness of the simulation. Network bursts occur because of the synchronization of firing neurons. Therefore, a decrease in the burstiness index is related to a decrease in synchronisation.
We quantify the decrease in feed-forward excitation by comparing the mean excitatory synapses in control simulations to simulations with acetylcholine. As these synapses decrease in strength, the excitatory neurons are less likely to excite other neurons, showing a decrease in feed-forward excitation.
The magnitude of Long Term Potentiation (LTP) is assessed by logging the absolute value of each STDP update in simulations. This value is equal to the value of ΔS in equation 2.7. To correct for the difference in the amount of STDP updates, a probability distribution is calculated for each simulation. The Euclidean Distance ED is used to quantify the ability to consolidate memory. More information on ED can be found in several paragraphs above.

Mutual Information

In information theory, information is described as the reduction in uncertainty in one variable when another variable is known [37]. So, if learning the state of one variable reduces the uncertainty in another variable, then the first variable provides information about the second variable. It is possible to quantify uncertainty using entropy, so a reduction in uncertainty can be quantified as information.
If we declare two variables X and Y, then the total entropy of X is equal to the entropy that remains in X after Y plus the information $I(X;Y)$ provided by Y about X. Therefore, we can write for the total entropy $H(X)$:

$$H(X) = H(X|Y) + I(X;Y) \tag{2.10}$$

This equation can be rearranged and rewritten using the probability density function (see 2.11), thus getting an expression for mutual information. The information will be measured in bits since entropy has also the unit of bits [37].

$$I(X;Y) = H(X) - H(X|Y) = \sum_{x \in X, y \in Y} p(x,y) log_2 \left(\frac{p(x,y)}{p(x)p(y)} \right) \tag{2.11}$$

For this analysis, the variable X denotes the times at which electrical stimulation is applied and Y is defined as the action potentials from a particular neuron. To decrease computational time, both signals are binned with a bin size of 100 ms. For X, bins with a stimulus are set to 1 and other bins are 0. For Y, bins with one or more action potentials are set to 1 and all other bins are set to 0, so there is no discrimination between the number of firings in each bin.
With prediction, we are interested in the amount of information that the firings of neurons give about the stimuli. Therefore, we investigate the MI between Y and time-shifted values of X. The range of time shifts is from 100 ms after a stimulus, to quantify the stimulus-response until 3000 ms before the actual stimulus is given, to quantify prediction.
Per time shift, the MI will be calculated for each hour via the following paradigm. First, the neuron that gives the highest MI value between X and Y will be determined. We add each time another neuron if it increases the MI. We chose a maximum of five neurons since it was found that the largest sets do not give more information. If there is no option for a neuron that increases the MI, the current set will compute the last value for the MI of that hour and time-shift.

Statistical analysis

The results are all shown as the mean and standard error of the mean. The statistical analysis was performed in SPSS (IBM, New York, USA), where a significance level of 5 % was used. In line with Dias et al., the homogeneity of variances and normal distribution of the residuals is tested using Levene's test with a significance level of 5 %, a Shapiro-Wilk test and Q-Q plots [2]. With normally distributed data, two-sample t-tests, one-way repeated measures ANOVA or two-way repeated-measures ANOVA were used. For non-normally distributed data, a Wilcoxon test was applied. If there were multiple pair-wise comparisons, the significance threshold was corrected with the Bonferroni correction. For each test, the corresponding p-value.

Chapter 3

Results

In this chapter, we describe the results from simulations that are described in section 2.1.3. In the first part, we look at the development of the network, validate activity patterns to *in vitro* data and investigate the effect of activity homeostasis on memory consolidation. Next, the results from the validation of acetylcholine (ACh) are given. In the final section, we will show the results of the mutual information analysis on prediction.

3.1 Validation

3.1.1 Simulations with activity homeostasis

Figure 3.1a displays the Euclidean Distance (ED) of the synaptic matrices of a representative simulation with respect to t= 0 h for the first nine hours of the simulations. The ED displays the magnitude of change of all synaptic strengths. In this particular figure, one should focus on the slope of the line. A steep slope indicates many changes in synaptic strength over time, whereas a flat line indicates few changes. For the first hours, the slope of ED is steep, which signals that there are many changes in the strength of synapses. Over time, the slope of ED is decreasing, indicating that the magnitude of change over time is decreasing as well. From t= 5 h to t= 6 h, the line is nearly flat, indicating that synaptic strengths are hardly changing. Therefore, six hours is used as 'development time' for the network. At t= 6h, stimulation is applied, which disrupts the line. However, the line flattens out over time to a slope that is similar between t= 5h and t= 6h.
Activity homeostasis acts on synapses, yet it is unknown how this affects the synaptic strengths. In figure 3.1b, the distribution of excitatory synapses (these are the only plastic synapses) is plotted after six hours of spontaneous activity for a representative simulation with- and without activity homeostasis. Both have developed a bi-modal distribution, with peaks at the minimum and maximum synaptic strength. However, for the distribution with activity homeostasis, small numbers of synaptic strengths are spread out over the distribution.
A burst-dominated firing pattern is one of the distinct properties of cortical cultures. Therefore, we need to validate if the model can represent this. Panel (c) and (d) both display both raster plots, for *in silico* data and *in vitro* data respectively. In both top panels, five minutes of spontaneous activity is plotted for each recorded neuron, whereas the bottom panel displays a single burst. Both top panels display a burst dominated firing pattern, as neurons fire synchronously. However, there are some differences visible. The amount of bursts in the *in silico* data is larger and each neuron has similar activity, whereas the activity of neurons in the *in vitro* data are more spread out. Some neurons are more active, like neurons 37, 52 and 55. Whereas others fire sporadic, like neuron 15.
Both bottom panels display a representative single burst, which also shows some differences. The burst duration of the *in silico* data is approximately 40 ms, whereas the burst of the cortical culture is almost 150 ms. The *in silico* burst has a constant intensity over time and abruptly stops, whereas the *in vitro* burst fades out from a high intensity of spikes.

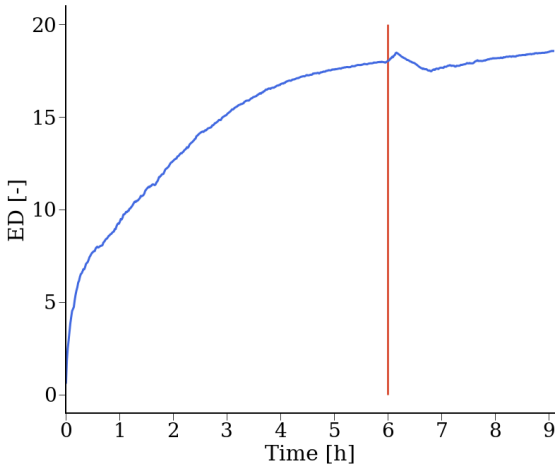

((a)) The blue line denotes the euclidean distance of the synaptic matrices over time with respect to t = 0 h. The scope is the slope of ED over time. The slope of ED is first steep but decreases over time. Between t = 5 h and t = 6 h, the line is nearly flat, indicating that synapses experience little change. Therefore, t = 6 h is chosen as the beginning for stimulation. The red line in the figures denotes the beginning of stimulation. This disrupts the line. However, the slope of the line returns to similar values as for t $\leq$ 6 h.

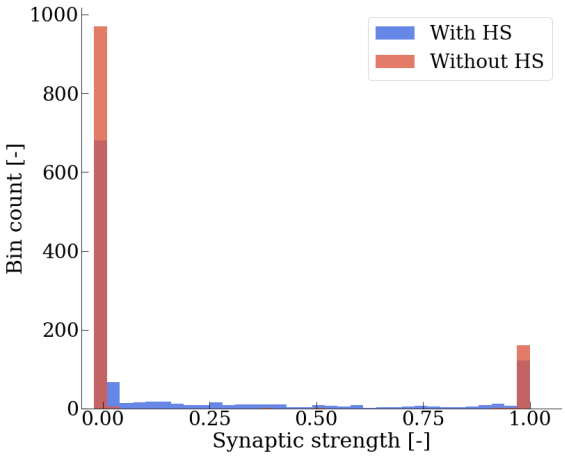

((b)) Distribution of all excitatory synapses during spontaneous activity after the network has found a balance in activity and connectivity (t = 6 h). For the simulation without activity homeostasis (red), all values are in the bins at the minimum and maximum of the possible values for the synaptic strength, 0 and 1 respectively. Most synapses in the simulation with activity homeostasis are also present in these bins. However, a small amount of the synapses are uniformly distributed across the possible values for the synaptic strengths.

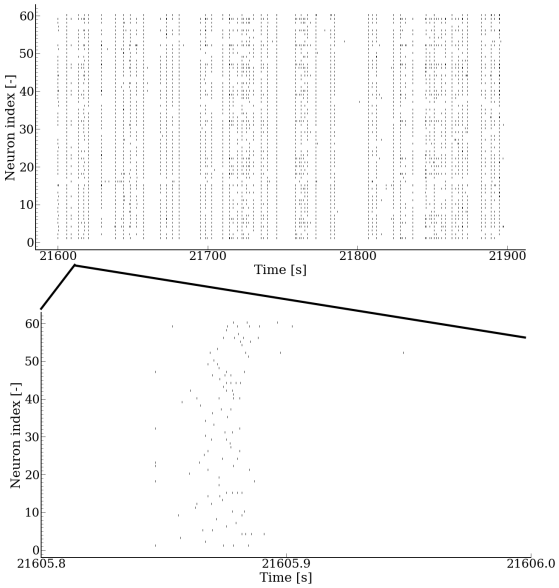

((c)) Top panel: Raster plot of five minutes of spontaneous activity of an *in silico* network after six hours of intrinsic activity. A synchronised firing pattern is visible with little activity between network bursts Bottom panel: Zoom of a raster plot of a representative single burst. The duration of the burst is approximately 40 ms, the burst starts with a few spikes and quickly intensifies after which it abruptly stops.

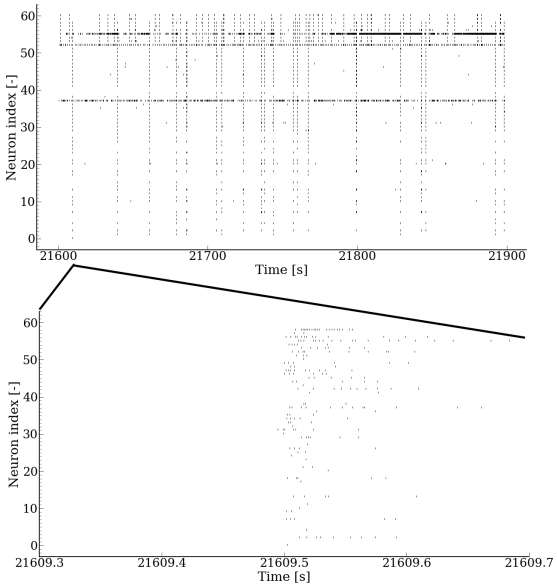

((d)) Top panel: Raster plot of five minutes of spontaneous activity of an *in vitro* network after six hours of intrinsic activity. The firing pattern is synchronised with little activity between network bursts. The activity of neurons is more heterogenous as *in silico*, where most neurons have the same activity. Bottom panel: Zoom of a raster plot of a representative single burst. The burst quickly intensifies and fades slowly out over time.

Figure 3.1: Overview of the results used for the validation of control simulations. Panel (a) displays the Euclidean Distance of the synaptic matrices from the initialisation of the network. Panel (b) shows the distribution of excitatory synapses for both simulations with- and without activity homeostasis after the network has found a balance in connectivity and activity. In panel c, two raster plots are displayed that show the neural activity of a simulation for five minutes and during a single burst. Panel (d) displays similar raster plots, but for *in vitro* data.

Memory consolidation

The Euclidean Distance (ED) is used to quantify memory consolidation. In this case, ED indicates how much synaptic strengths have changed after stimulation. Figure 3.2 displays ED for the memory consolidation experiments with activity homeostasis (blue) and without activity homeostasis (purple). The focus in this analysis will be mostly on the shape of the curves, as this displays how the network is changing over time.
In the first stimulation sequence with stimulation set A (t = 1-4 h), a similar pattern is visible for simulations with- and without activity homeostasis. Each hour, the value of ED increases, but the magnitude of change decreases over time. This indicates that after each period of stimulation, synapses are less changing.
This pattern is also visible for simulations with activity homeostasis for stimulation set B (t = 5-8 h). However, for simulations without activity homeostasis a different pattern is present. The value for ED is small and the curve is linear. It indicates that the stimulation does not induce as many changes in synapses.
For the last four hours of the simulation, the network is stimulated with stimulation set A again. For both simulations with- and without activity homeostasis, ED is small for each hour. It indicates that synaptic changes are present, but the magnitude of these changes is less than stimulation for the first time with stimulation set A (t = 1-4 h).

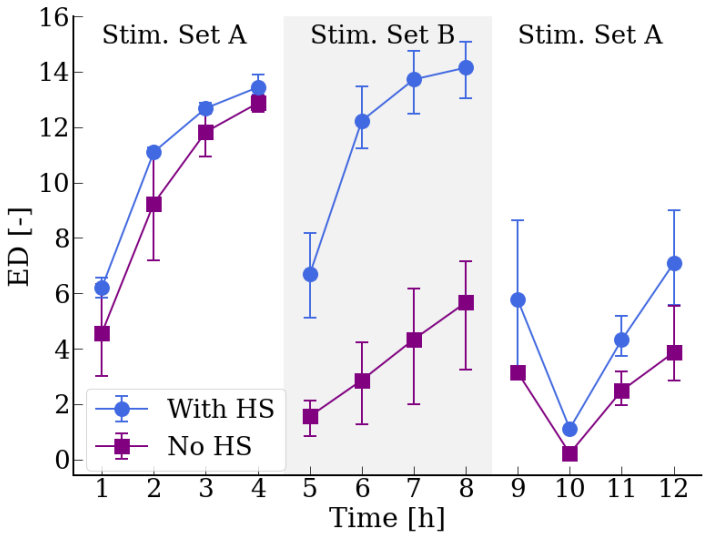

Figure 3.2: Euclidean distances ED between synaptic matrices for simulations with activity homeostasis (blue) and simulations without activity homeostasis. The figure displays the results of the memory consolidation experiments in which low-frequency stimulation was applied. For the first four hours, a similar pattern is found for both conditions. Each hour the value of ED increases, but the magnitude of change decreases each hour, resulting in a line that flattens over time. In hours 5 - 8 h, a different set of neurons is stimulated. During these hours, a difference is visible between the two conditions. For the simulations with activity homeostasis, the same pattern is found for stimulation with set A. However, without activity homeostasis, ED is small for each hour and a linear increase is visible. For the remaining hours, set A is stimulated again. For both conditions, ED is small for each hour and the pattern does not resemble any pattern in the previous hours.

3.1.2 Validation of the effects of acetylcholine

Firing rate

This section describes the validation of the effects of acetylcholine with *in vitro* data. We validate the increase in firing rate, dispersed firing, decreased synaptic strengths and the hampering of memory consolidation to the findings of Dias et al. [2]. Each time the *in silico* data is shown on the left side and the *in vitro* data on the right side. Each figure corresponding to *in silico* data has displays values for ACh (acetylcholine) and control, in which control is the model including activity homeostasis. The *in vitro* figures display values for control and CCh, where CCh denotes carbachol, an acetylcholine antagonist.
Figure 3.3 displays the mean firing rate during memory consolidation experiments for *in silico* simulations and cortical cultures. Both situations with- and without acetylcholine (control) are plotted. For this analysis, the magnitude of the values is the most important. For *in vitro* data, statistical tests have found that the firing rate with CCh is higher than in control experiments. In the figure, it is visible that the firing rate is each hour higher. The same applies for the *in silico* data, each hour the firing rate is higher for simulations with ACh and a statistical difference has been found.

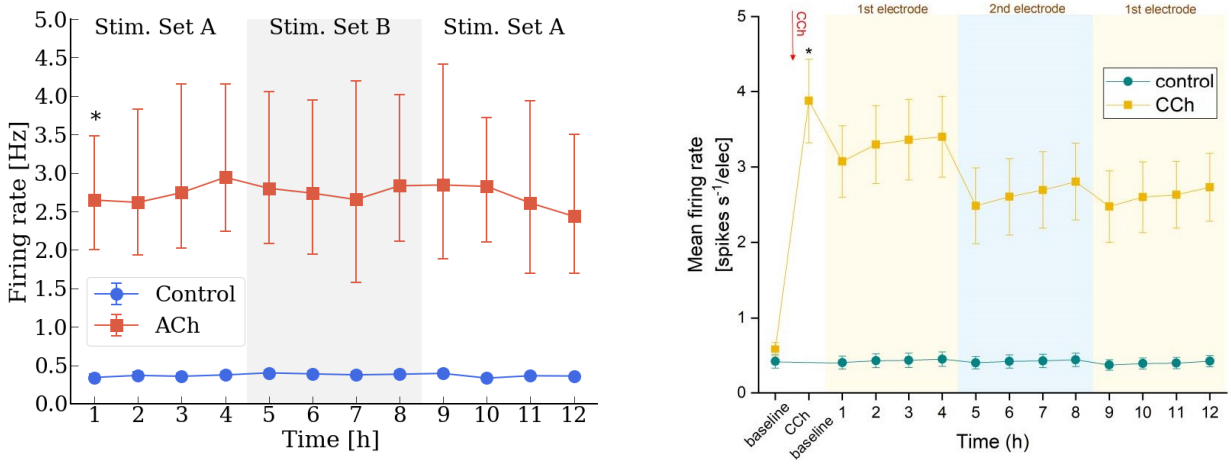

Figure 3.3: Mean Firing Rate (MFR) for *in silico* (left) and *in vitro* (right, obtained from [2]) experiments. In both panels, the MFR is given for control experiments and experiments with ACh/CCh. For *in vitro* data, the MFR for experiments with CCh is each hour significant higher than in control experiments. The *in silico* data displays the same difference.

Dispersed firing

The next step in the validation is to verify whether the dispersed firing pattern is present. Figure 3.4 displays five minutes of spontaneous activity for a realization with activity homeostasis (a), *in vitro* data (b) and a realization without activity homeostasis (c).
Panel (b) is the reference in this analysis, as this panel shows the *in vitro* data. Network bursts are not visible and neurons fire with low synchronicity. The same pattern can be seen in panel a. There is an absence of synchronicity, with no network bursts. However, there are some differences. Panel (a) displays short periods of activity for most neurons over time and two neurons fire with high intensity over a long period (black horizontal stripes), whereas in panel (b) most neurons fire more continuously over time. Panel (c) displays a realization without activity homeostasis. It is visible that neurons fire with high synchronicity as network bursts are present.

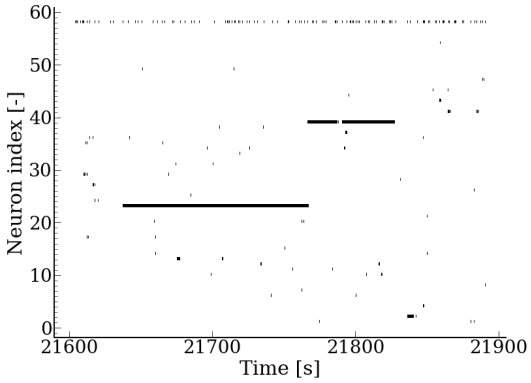

((a)) *In silico* model with activity homeostasis

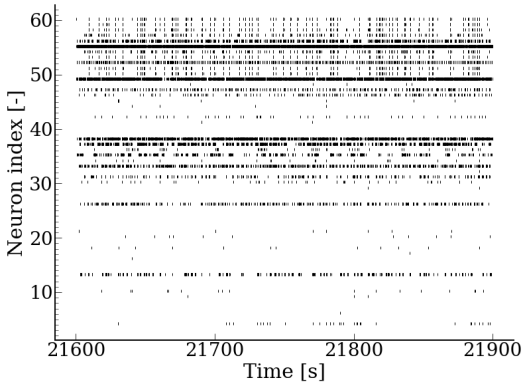

((b)) *In vitro* cortical culture.

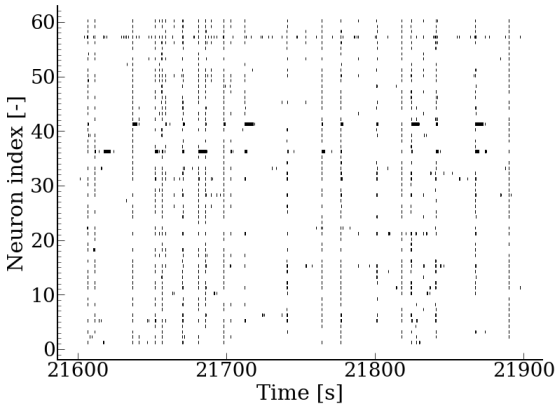

((c)) *In silico* model without activity homeostasis.

Figure 3.4: Each raster plot displays five minutes of spontaneous activity with ACh (or CCh *in vitro*), every dot in the plot represent an action potential. Panel (a) corresponds to a simulation with activity homeostasis, panel (b) to *in vitro* data and panel (c) represents a simulation without activity homeostasis. (b) displays that neurons are firing without synchronicity, with an absence of network bursts. The activity of the neurons is heterogeneous as some neurons are more activity than others. Panel (a) displays the same absence of synchronicity for a simulations with activity homeostasis. Some neurons become very active for a certain amount of time (black horizontal lines). In simulations without activity homeostasis (c), the activity pattern displays network bursts and neurons that fire in synchronise.

We validate the dispersed firing pattern also in a quantitative matter, namely with the Burstiness Index (BI). The scope of this analysis is to prove a difference between the BI of control simulations and simulations with ACh. Figure 3.5 displays both *in silico* and *in vitro* results of the BI in control experiments and experiments with ACh. The *in vitro* data display a clear difference between control and CCh. With CCh, the value for BI is each hour statistically lower than for controls. For *in silico* data, we see the same behaviour as the BI for simulations with ACh is lower for each hour and a statistical difference has been found.

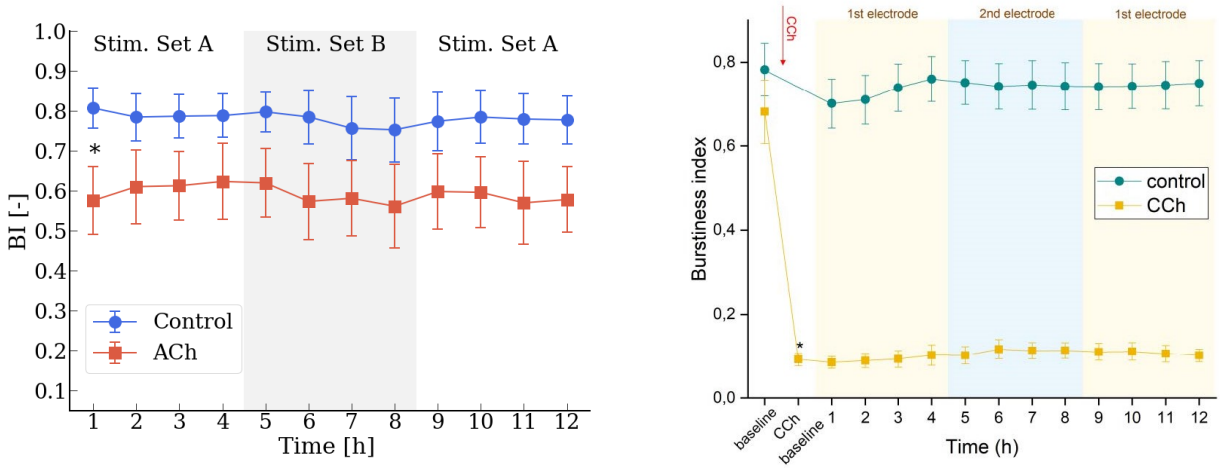

Figure 3.5: Bustiness Index (BI) for both *in silico* data (left) and *in vitro* data (right, obtained from [2]). In both panels, the BI is plotted for control experiments and experiments with ACh/CCh. The right panel displays a relatively large value for BI in control experiments with similar values for each hour. Experiments with CCh results in a significantly lower value for BI for each hour.
In silico, the BI for control simulations is also large, with similar values to the *in vitro* data. Also, a significant decrease in BI is found when ACh is included in the simulation. However, the decrease in BI is not as strong as for the *in vitro* data.

Synaptic strength

The next step in the validation, is to validate the decrease in synaptic strength by ACh. In figure 3.6, the synaptic strength is plotted for *in silico* data (left) and *in vitro* data (right) for both control experiments and experiments with ACh/CCh. The *in vitro* data display a decrease in synaptic strength if CCh is present. This difference between mean synaptic strength for control and experiments with CCh is significant. For the *in silico* data, the mean connection strength with ACh is for each hour lower than in control simulations with statistical differences.

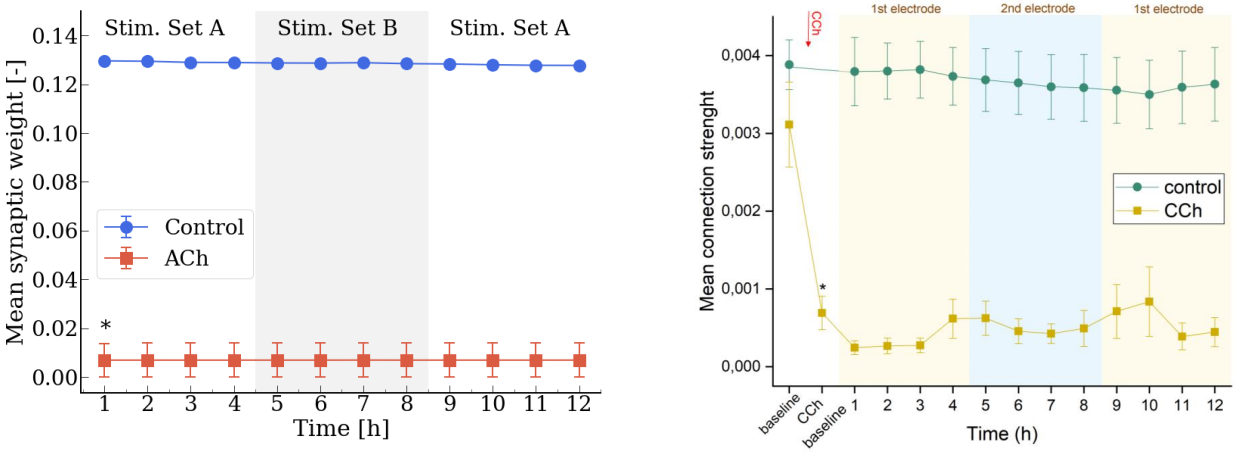

Figure 3.6: Mean Synaptic Weight for both *in silico* data (left) and *in vitro* data (right, obtained from [2]). In both panels, the mean synaptic weight is plotted for control expriments and experiments with ACh/CCh. The *in vitro* data displays a clear difference between both conditions, as the synapses are stronger in control experiments for each hour. The values for control experiments display little fluctuation over time, whereas the values for CCh are experiencing some fluctuation over time. The plot of the simulations (left) display the same difference. The synapses are stronger in control simulations. Unlike, the *in vitro* data, the values for ACh are not fluctuating.

Long-Term Potentiation

For the next validation, there is no *in vitro* data available, as this is not possible to measure STDP changes *in vitro*. In Figure 3.7, the distribution of the magnitude of STDP in control simulations and simulations with ACh is given. The maximum value of the STDP update is 0.005. During memory consolidation experiments, each STDP update was logged. In the left plot (control), each magnitude of STDP update has approximately the same probability. For simulations with ACh, a unimodal distribution has formed. For values smaller than 0.004, the probability is close to 0. The probability between 0.004-0.005 (the maximum value) is high. This implies that for each STDP update, the change in synaptic strength is relatively large.

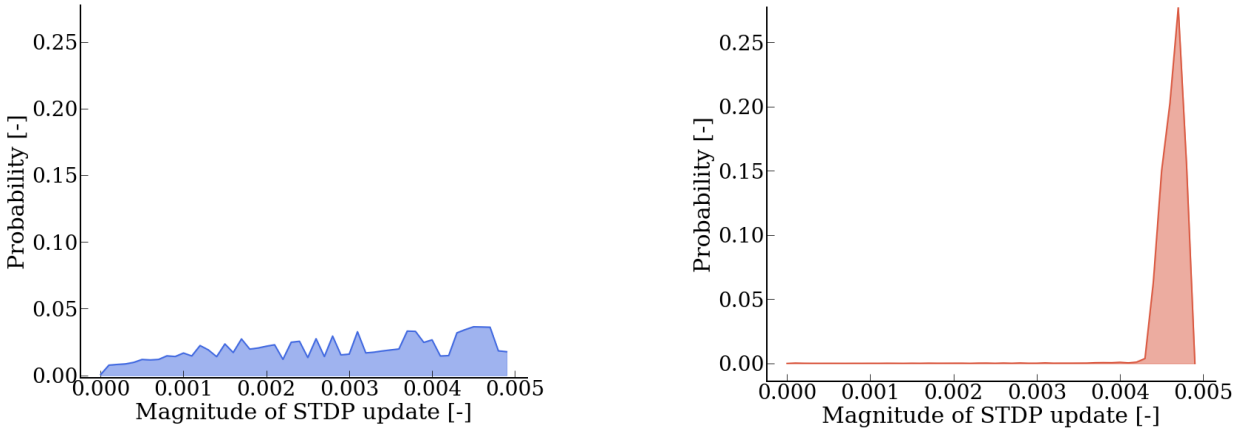

Figure 3.7: The probability distribution of the magnitude of the STDP update rule for control simulations (left) and simulations with ACh (right). The probability distribution is visualized between the minimum value (0) and maximum value (0.005). For control simulations, a uniform distribution is visible. It implies that each value is as likely to occur as any other value. For ACh, a different distribution is visible. For the values smaller than 0.004 the probability is nearly zero, a small value for an STDP update is implausible. A peak has formed between 0.004 and 0.005. With ACh, synapses are experiencing larger changes by STDP.

Stimulus response

Before we validate the effect of ACh on memory consolidation, the stimulus responses will be analyzed to make sure that the networks are properly stimulated in both control simulations and simulations with ACh. In 3.8a, the stimulus-response is given for control simulations. After stimulation is applied (red arrow), a peak is visible, indicating that many neurons are firing. After 40-50ms, the peak has disappeared. In the first section of the results, it was found that bursts in simulations last around 40 ms. Therefore, it is likely that the stimulation induces a network response.
In the right plot (b), the stimulus-response is given for simulations with ACh. After stimulation is applied, the bin count increases and slowly decreases over time. As this bin count sharply increases after the red arrow, a stimulus-response has likely occurred.

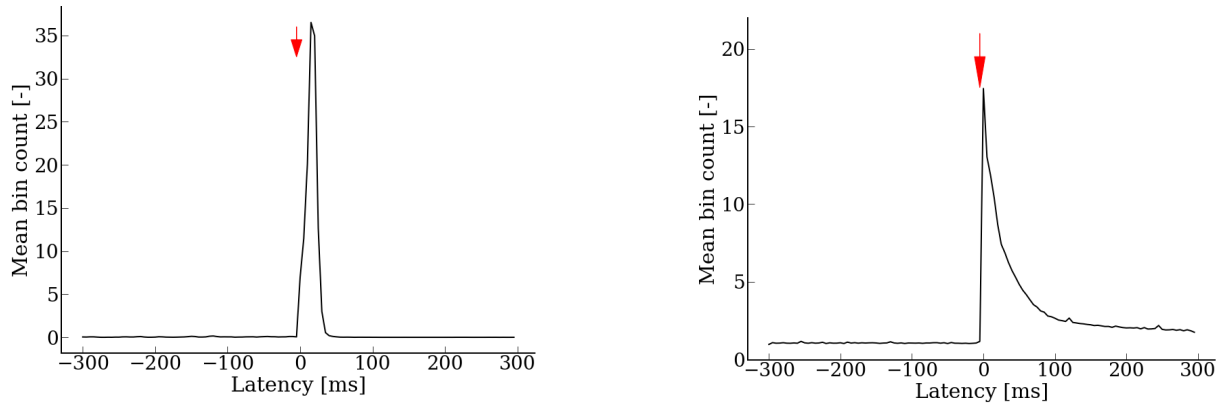

Figure 3.8: Stimulus response curves for control simulations (left) and simulations with acetylcholine (right). The bin count denotes the mean amount of spikes per 5 ms. The red arrow is placed at the moment that a stimulus is applied (latency = 0 ms). In both panels, a rise in bin count is visible when the stimulus is applied. For control simulations, the peak value is larger, but the width of the peak is smaller. The values after the peak in control simulations are similar to values before the stimulus, whereas in simulations with ACh these bin counts are larger.

Memory consolidation

Last, it will be validated if the model can reproduce the hampering of memory consolidation in simulations with ACh. Memory consolidation is quantified with the Euclidean Distance ED of the synaptic matrices. The ED for *in silico* data is given in the left panel of Figure 3.9 and the right panel displays *in vitro* data. In this analysis, we focus on the shape of the curves as they display the amount of change over time in synaptic strengths.
The *in vitro* data displays for hours 1-4 and 5-8 an increase in ED for each hour with a decreasing magnitude of change over time. Stimulation of the first electrode for the second time (t = 9-12 h) results also in an increase in ED. However, the magnitude is smaller, such that for each hour the difference between the baseline measure is non-significant.
For the *in silico* data, similar behaviour is seen for hours 1-4 and 5-8. Each hour the value of ED increases, but the line flattens over time. Returning to the first stimulation set results in a different pattern. The values are small each hour and the curve is not flattening over time.
For *in vitro* experiments with CCh, values for the ED are lower than in control experiments and are fluctuation over time, instead of the distinct curves present in control data. The ED for *in silico* simulations, display a low value for each hour with no fluctation over time.

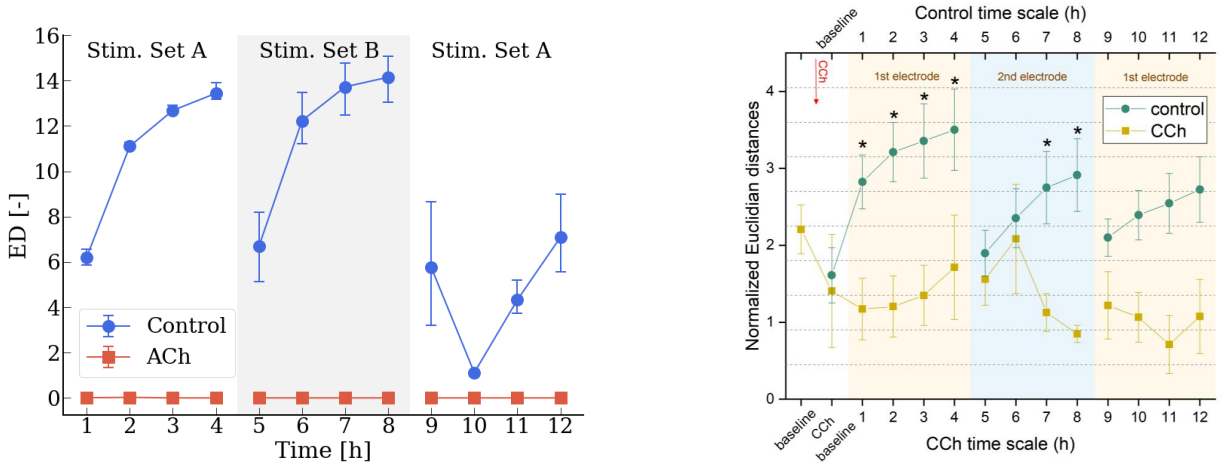

Figure 3.9: The Euclidean Distance ED in memory consolidation experiments is visualized for *in silico* data and *in vitro* data (right, obtained from [2]). In both panels, data is visualized for control experiments and experiments with ACh/CCh. For control experiments *in vitro*, ED increases each hour for hours 1-4 and 5-8. However, the magnitude of change decreases each hour. This behaviour is also present *in silico*. The stimulation of the first electrode for the second time results in a small increase in ED in each hour such that it is not significantly higher than the baseline value for ED. The left panel displays a different behaviour, ED is small for hours 9-12, but it does not increase each hour.
In vitro experiments with CCh, display a small value for ED each hour during the whole experiments, with some fluctuations. The values for ED in the *in silico* experiments are also small, but no fluctuations are visible.

3.1.3 Sensitivity analysis

Figure 3.10 display raster plots for the sensitivity analysis. The goal of this analysis is to investigate to which extent variation of the chosen parameters affects the firing pattern present with ACh.
The first row displays a decrease (left) and increase (right) of the time constant of activity homeostasis. Both figures show dispersed firing as the synchronicity is low and network bursts are absent. Variation of the target of activity homeostasis (second row) does have the same effect, as dispersed firing is still present.
With the variation of the reset parameter of v for the Izhikevich neurons, a difference is present (panels (e) and (f)). A decrease (more negative) does result in network bursts, like for 21600 - 21720 s. However, periods with low synchronicity are also present (21750-21850 s).
Variation of the strength of the Inhibitory-Excitatory synapses does have little influence on dispersed firing, as a decrease and increase both results in a dispersed firing pattern (panels (g) and (h)). Finally, for an increased in parameter d of the Izhikevich neurons (panel (i)), the activity of the neurons is synchronized with no dispersed firing present.

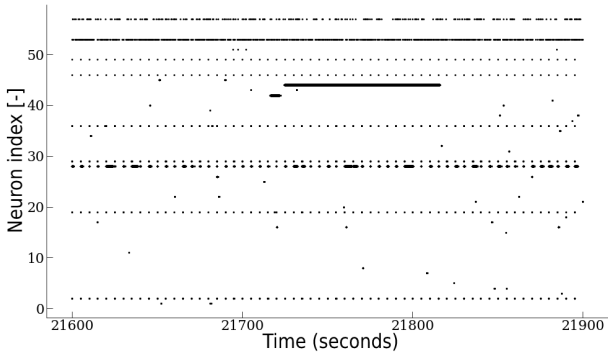

((a)) Decreased parameter τ_{HS} (i.e. time constant of activity homeostasis) by 10%.

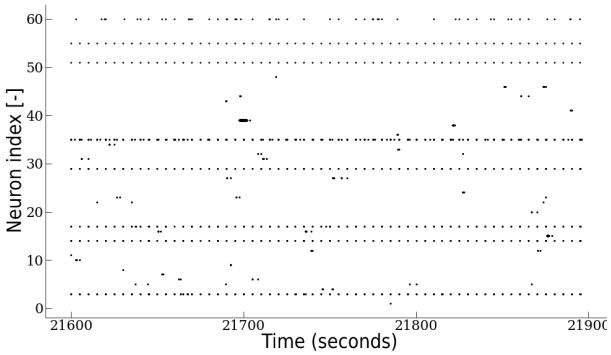

((b)) Increased parameter τ_{HS} (i.e. time constant of activity homeostasis) by 10%.

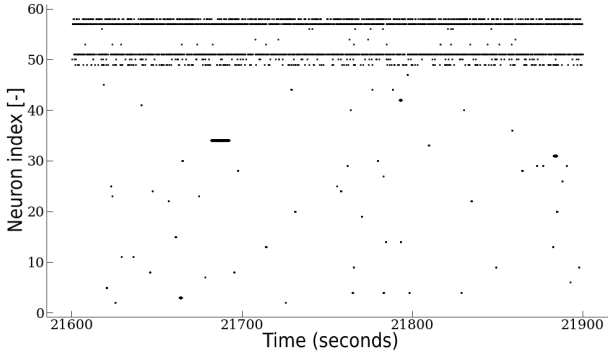

((c)) Decreased parameter $\hat{y}$ (i.e. target frequency of activity homeostasis) by 10%.

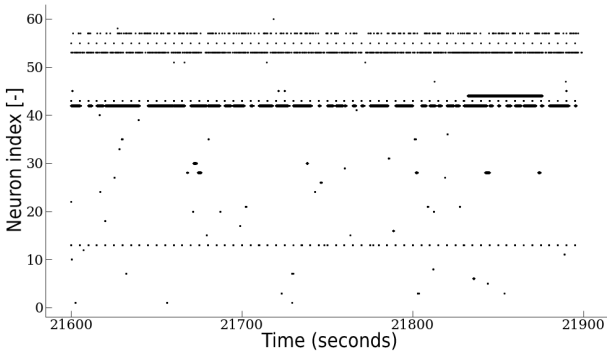

((d)) Increased parameter $\hat{y}$ (i.e. target frequency of activity homeostasis) by 10%.

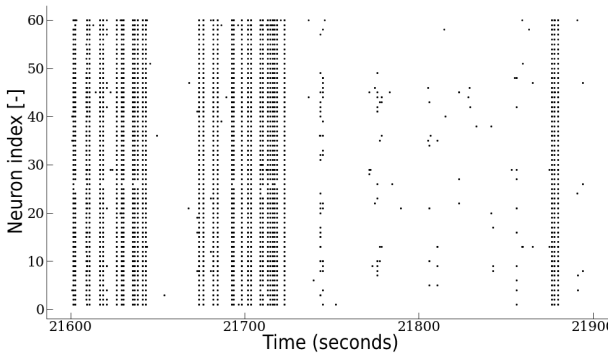

((e)) Decreased parameter c_{ACh} (i.e. reset parameter of v for the Izhikevich neurons) by 10%.

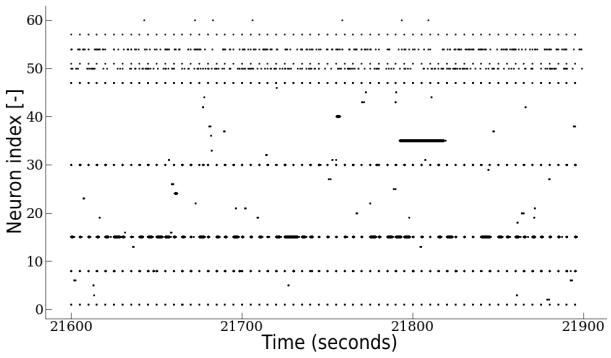

((f)) Increased parameter c_{ACh} (i.e. reset parameter of v for the Izhikevich neurons) by 10%.

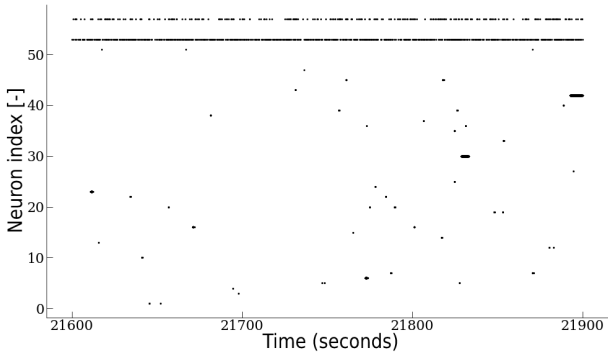

((g)) Decreased parameter IE_{ACh} (i.e. strength of Inhibitory-Excitatory synapses) by 10%.

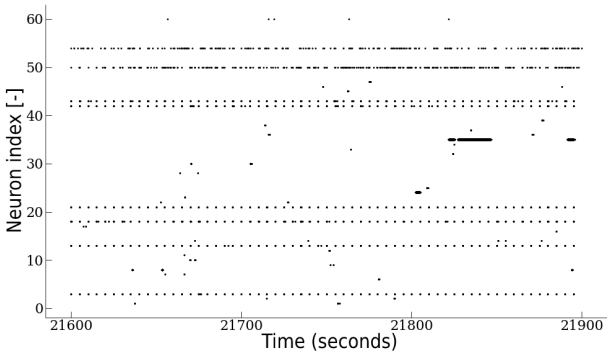

((h)) Increased parameter IE_{ACh} (i.e. strength of Inhibitory-Excitatory synapses) by 10%.

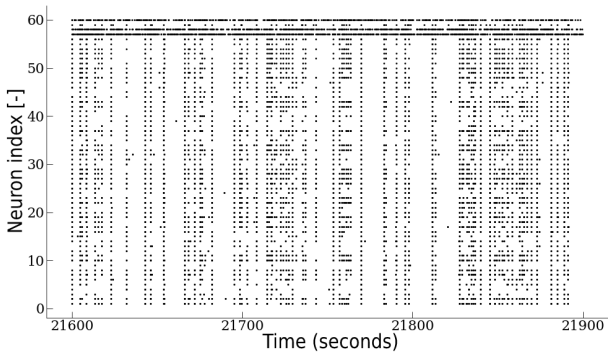

((i)) Increased parameter d_{ACh} (i.e. parameter for the strength of hyperpolarization after a spike of the Izhikevich neurons) by 10%.

Figure 3.10: Effect of parameter values for activity homeostasis and ACh on the firing pattern of simulations with acetylcholine. Each row represents variation in a different parameter, where the left column corresponds to a decrease in the value and the right column represents an increase in value. The raster plots show 5 minutes of activity after the network has found a balance in connectivity and activity.

3.1.4 Prediction experiments

The memory consolidation experiments involved repetitive stimulation in short periods. In prediction experiments, non-repetitive continuous stimulation is applied for twenty hours. In this section, it will be analyzed how the synapses change as a result of this continuous stimulation over time. The measure for this is ED, which is shown in 3.11 for each hour of the prediction experiment. A large increase in ED is present during the first two hours, after which the line flattens for the remainder of the experiment.

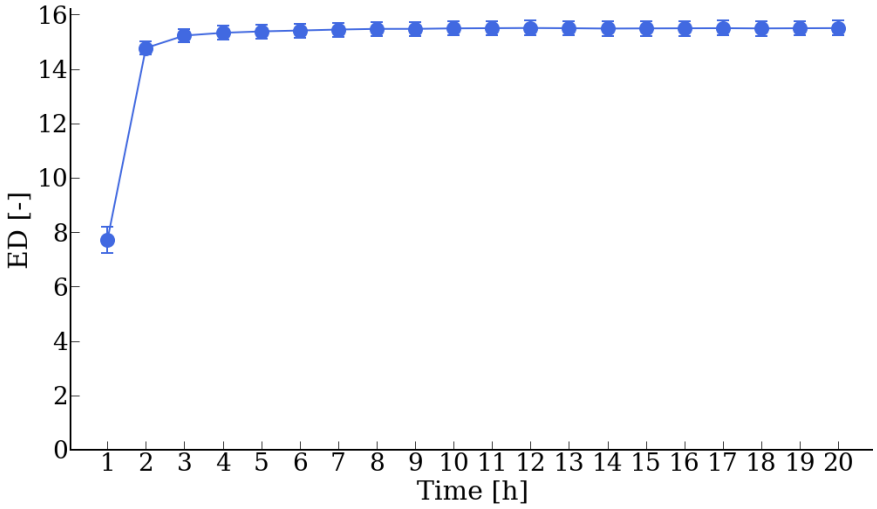

Figure 3.11: The Euclidean Distance ED of the prediction experiments with respect to the beginning of the stimulation. In the first two hours, ED strongly increases, representing many changes in synapses. After several hours, the value of ED stabilizes and remains the same for the rest of the experiment.

3.2 Prediction

Before we examine the *in silico* results, it is important to validate the finding of Mutual Information (MI) with *in vitro* data. In the experiments, the stimulations have been shifted in time. Therefore, we will focus on the value of MI over these shifts in time (i.e. stimshifts). Figure 3.12 displays the MI of *in silico* data (left) and *in vitro* data (right). For stimshifts smaller than 1000 ms, both panels show a plateau for MI. At 1000 ms, both plots display a peak, after which MI decreases until 2000 ms. At 2000 ms, a small increase in MI is present for both *in silico* and *in vitro* data. Both panels are very similar, with the only noticeable difference being the height of the peak at 1000 ms. This peak is larger for *in vitro* data than *in silico* data.

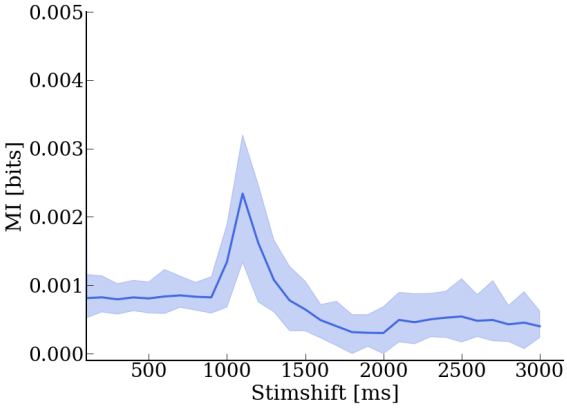

((a)) Mutual Information for *in silico* data. A plateau forms for stimshifts smaller than 1000 ms, after which a peaks forms and gradually decreases until 2000 ms. At this stimshift a small increase in MI is found for the remainder of the figure. The shape of the plot is similiar to *in vitro* data, but the peak at 1100 ms is smaller.

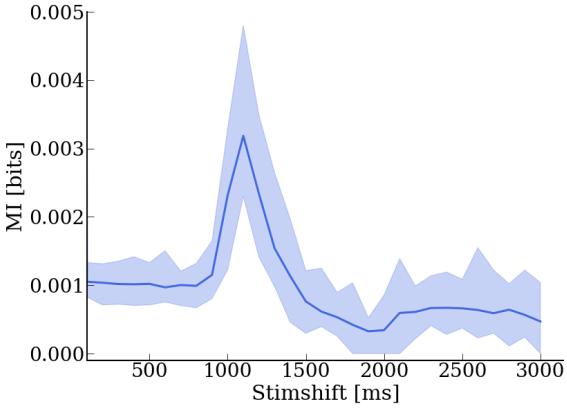

((b)) Mutual Information for *in vitro* data. A plateau forms for stimshifts smaller than 1000 ms, after which a peaks forms and gradually decreases until 2000 ms. At this stimshift a small increase in MI is found for the remainder of the figure. The shape of the plot is similiar to *in silico* data, but the peak at 1100 ms is larger.

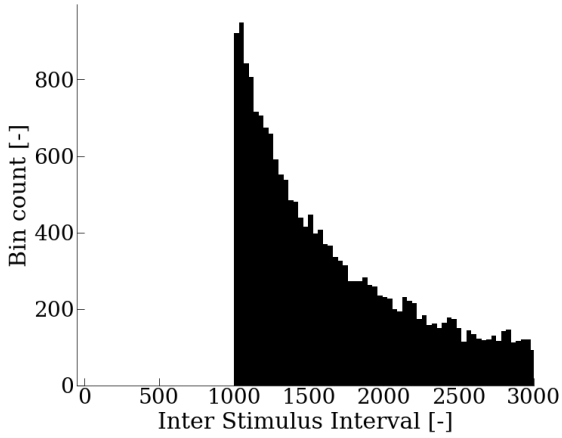

((c)) Inter-Stimulus interval (ISI) distribution used in the experiments that gave the results of plots (a) and (b). It is interesting to note that the minimum ISI corresponds to the end of the plateau in the plots of MI above and that the peak in MI corresponds to the most probable ISI.

Figure 3.12: Panel (a) and (b) show the results of the MI analysis for *in silico* and *in vitro* respectively. The used ISI distribution is shown in panel (c).

Figure 3.13, displays the mutual information (MI) for each hour over time-shifted stimulation patterns, which we call *'stimshifts'* in this analysis. Negative stimshifts indicate that stimulation precedes activity and positive values denote that neural activity preceded stimulation. Each time, the plot on the left shows MI with this corresponding ISI distribution, as the ISI distribution has been modified for analysis. The line in the MI plots corresponds to the mean value of all hours and the edges of the coloured region are the minimum and maximum value for MI at that particular stimshift.
Panel (a) shows the MI for stimshifts in the range of -100 to 3000 ms. The largest values are at stimshifts of -100 and 0 ms. These values mask the behaviour that is present in panel (c). This figure displays the same results, but with the exclusion of stimshift -100 and 0 ms.
A plateau forms in (c) until a stimshift of 1000 ms. The end of this plateau coincides with the minimum ISI from the distribution of (d). MI gradually increases until the stimshift of 2000 ms, after which it strongly increases and peaks at 2100 ms, which coincides with the most probable ISI value (see (d)). The value for MI decreases for the remainder of the plot, with a similar slope to the ISI distribution. It seems as the values of MI depend on the ISI distribution, to verify this dependency we subtract all ISIs by 500 ms and check whether this dependency still exists.
This modification results in the ISI distribution shown in (f), with the plot of MI in panel (e). Again, a plateau forms for stimshifts smaller than the minimum ISI value, after which MI decreases and forms a low plateau. MI peaks at a value of 1600 ms, which coincides again with the most probable ISI. The value decreases with a slope similar to the ISI distribution as far as values before the peak. Figure (e) is similar to (c), with the obvious exception that all values are shifted 500 ms to the left. However, in panel (c) a slight increase is visible in the region of 1000-2000 ms, whereas in panel (e) MI forms a plateau from 500 to 1500 ms.
The MI values seem to rely on the distribution of the stimulations. However, it is not known if the stimulation responses themselves are the cause or the inter-stimulus neural activity. All bins corresponding to stimulus responses are randomly set to 0 or 1 to make them unrecognizable. This leads to the plot of (g), with no modifications to the ISI distribution. For each stimshift, the MI is low and the shape of the figure does not resemble previous plots. As all MI values are reduced, it is apparent that stimulus responses provide the most MI.

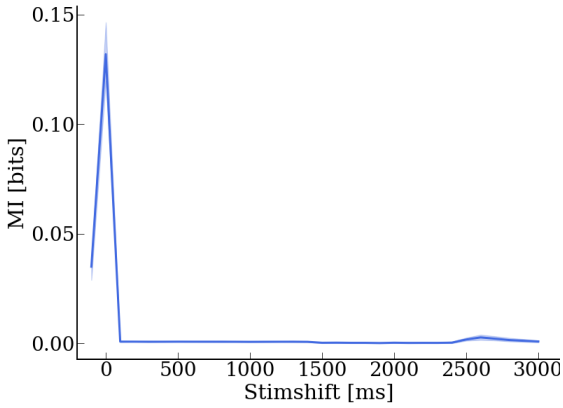

((a)) Mutual information for each hour and each time-shifted stimulation sequence from -100 until 3000 ms for the original neuron firings. It is clear that the largest values are found at stimshifts -100 and 0 ms, such that they mask the shape of the signal for larger stimshifts (like in (c)). Therefore, the analysis will only focus on stimshifts 100-3000 ms.

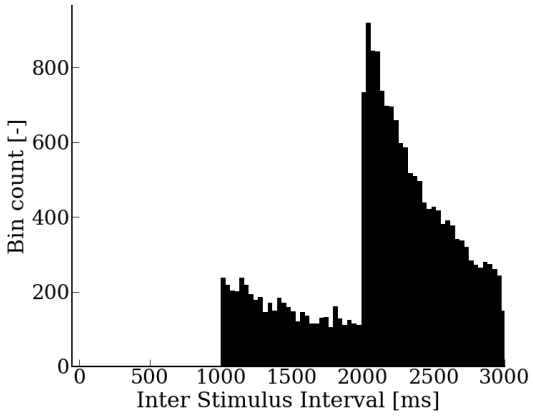

((b)) Corresponding inter-stimulus interval distribution.

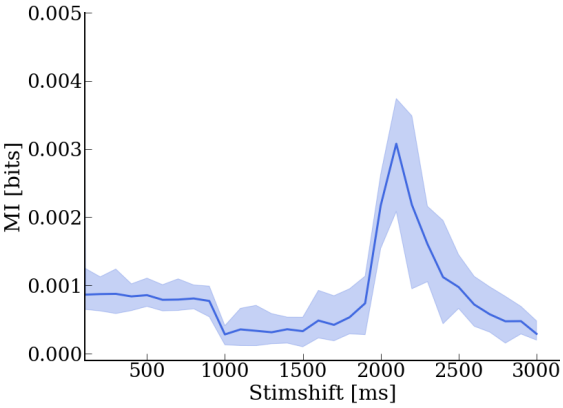

((c)) Mutual information for each hour and each time-shifted stimulation sequence from 100 until 3000 ms for the original neuron firings. A plateau forms for stimshifts that are smaller than the minimum ISI (see (d)), after MI decreases and slowly increases until 2000 ms. The peak forms at the most occuring ISI (2100 ms), after which MI decreases for the remained of the plot.

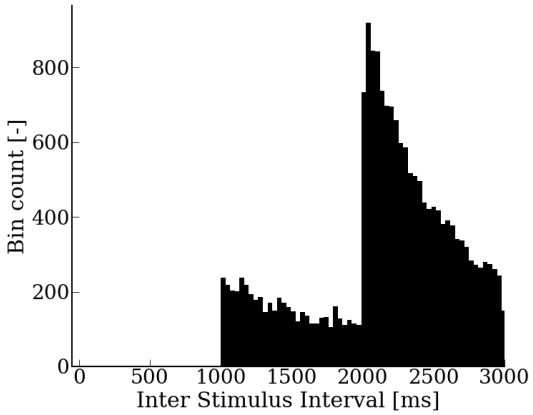

((d)) Corresponding inter-stimulus interval distribution.

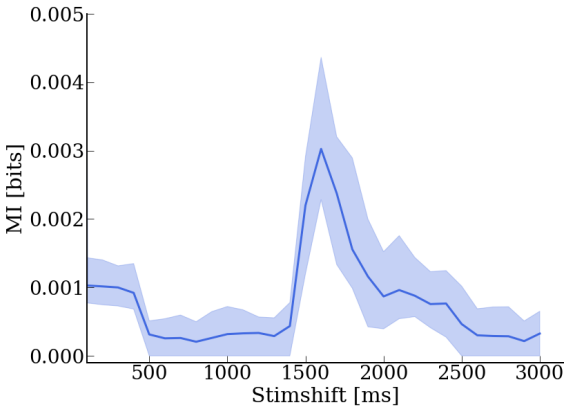

((e)) Mutual information for each hour and each time-shifted stimulation sequence from -100 until 3000 ms for the original neuron firings and subtraction of each ISI by 500 ms. Like in panel (c), a plateau in MI forms until the minimum ISI (500 ms). MI remains low until the most probable ISI, at which a peaks forms. The value decreases for larger stimshifts down to values as before the peak. The shape is similar to (c), but shifted 500 ms to the left.

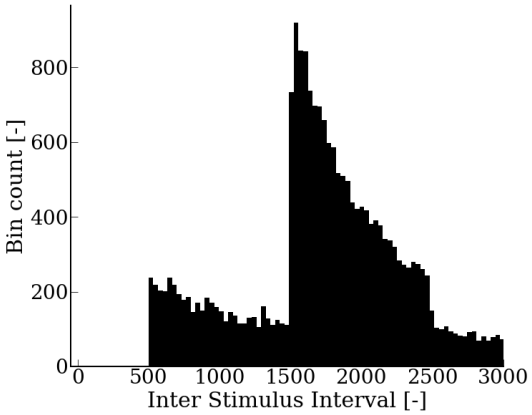

((f)) Corresponding inter-stimulus interval distribution. All ISIs have been reduced by 500 ms compared to (e), such that the minimum value is 500 ms and the most probable ISI is 1500 ms.

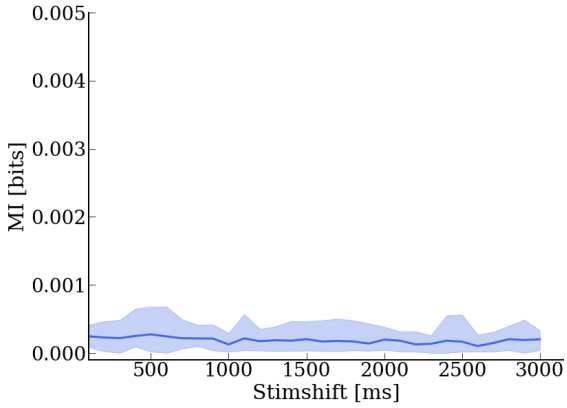

((g)) Mutual information for each hour and each time-shifted stimulation sequence from -100 until 3000 ms in which bins with stimulus responses are randomly set to zero or one. This analysis aims to see if the stimulus responses provide MI or that inter-stimulus activity also adds MI. For all stimshifts, MI is low and both indicators from previous figures (minimum ISI and most probable ISI) have disappeared.

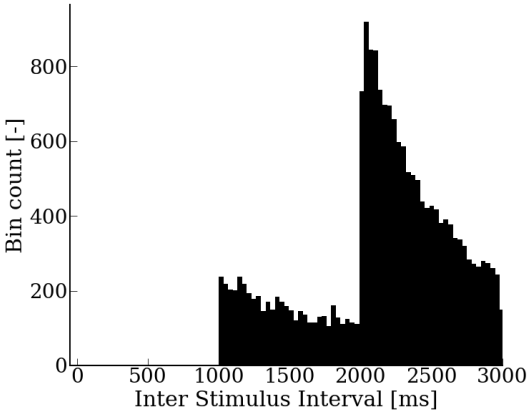

((h)) Corresponding inter-stimulus interval distribution.

Figure 3.13: Each row displays the MI over stimshifts (left) with the corresponding ISI distribution. For every row, a modification has been applied to either the activity of neurons or to the ISI distribution. The first and second rows (a-d) display the same results, but with a different range for the stimshifts. In the third row, all ISI values have been subtracted by 500 ms and in the last row, all bins with stimulus responses are randomly set to 0 or 1.

Chapter 4

Discussion

4.1 Changes to computational the model

4.1.1 Activity homeostasis

Activity homeostasis comprises of multiple nested mechanisms that control, for example, the number of synapses, the strength of synapses and intrinsic excitability [21]. We chose to only include synaptic scaling (i.e. regulating by adjusting synaptic strengths) to reduce complexity. If a network becomes too active, excitatory synapses are downregulated and/ or inhibitory synapses are upregulated. However, in our implementation, only excitatory synapses are adjusted.
This mechanism was added to the model by setting a target frequency and adjusting the synaptic strengths based on the difference between the actual firing frequency of the network and the target frequency. We set the firing frequency to the mean firing rate during normal conditions of *in vitro* cultures in the work of Dias et al. [2]. The mean firing frequency of neurons becomes close to the target frequency in simulations over time. It shows that synaptic scaling reaches its intended purpose.
Turrigiano found that activity homeostasis acts on a time-scale from hours to days [21]. This is a wide range and the choice for a time constant of eight hours is hard to justify as we chose it empirically. Furthermore, activity homeostasis comprises of multiple nested mechanisms in nature, which makes it hard to determine a single value for our simple implementation.
Moreover, the time constant of synaptic scaling is eight hours in the model, but the time-scale of acting was shorter (several minutes) compared to values described in the literature that range from hours to days [20]. Because of the small network size, a multiplication by a factor of six compensates for the synaptic strengths. Therefore, adjustments of synaptic strengths are also multiplied by this factor. This multiplication might explain the shorter timescale.
Future research should use larger networks such that less compensation is needed or the time constant of the activity homeostasis should be adjusted in the model. A bigger network is preferred, as this is more biologically plausible since *in vitro* cultures are composed of many more neurons than the 100 used in this thesis [15].

4.1.2 Acetylcholine

The starting point of this research was the model from the work of van Veenendaal and Dijkstra [18, 3]. This model could not reproduce *in vitro* results [3, 18] with acetylcholine (ACh) since it only increases neuronal excitability.

Parameter values

The action mechanisms of ACh were added to the model by adjusting the inhibitory-excitatory synaptic strength and two Izhikevich parameters that account for spike-frequency adaptation and the resting membrane potential. We increased parameters until a dispersed firing pattern was present and the mean firing rate resembled firing frequency of *in vitro* cultures. Results from the sensitivity analysis show that the model is sensitive to changes in the parameter c and d of the Izhikevich neuron. Settings for the strength of the Inhibitory-Excitatory and activity homeostasis had little influence on the firing pattern. Some figures from simulations of the sensitivity analysis were even more comparable to *in vitro* data as with the chosen parameters. Therefore, it is doubtful whether we have chosen the correct parameters. If feasible, a patch-clamp can record the membrane potential of neurons in conditions with ACh to fit the parameters of the Izhikevich neurons. Using the same validation as in this report, adjustments of the Inhibitory-Excitatory strengths can be varied until the desired values are found. In this thesis, we had to choose three parameters without direct measurements to validate. If the proposed method is feasible, only one parameter should be empirically determined, which will improve the reliability of the results. Furthermore, ACh affects K^+ channels and the Izhikevich neuron does not include these directly. However, the Hodgkin-Huxley neuron model does include these channels. We suggest to investigate replacing the Izhikevich neuron by the Hodgkin-Huxley model to improve the biological plausibility of the simulations with ACh0.

Validation

With synaptic scaling, synaptic strengths decreased in reaction to high neuronal activity. The low synaptic strengths resulted in reduced network excitability, which was reflected by the transition from burst-dominated activity patterns to dispersed firing. The addition of acetylcholine also enhanced synaptic plasticity, as showed by stronger STDP updates, which agrees with findings by Picciotto et al. who showed that ACh induces synaptic plasticity [11]. In agreement with experimental observations, the Burstiness Index (BI) decreased with high cholinergic tone. Although firing patterns in the *in vitro* and *in silico* data were dispersed, the BI in experimental recordings was much lower than in the computational model. Typically, neurons fire in short individual bursts in the computational model, whereas this is less pronounced *in vitro*. The BI depends on the distribution of action potentials. The individual bursts cause short periods of high activity, separated by periods of low activity, resembling the activity distribution over time of a burst-dominated pattern. This resemblance might explain the overestimation of BI.

Underlying mechanism

The validation with *in vitro* results of ACh confirmed the model is representative of cortical cultures. Dias suggested STD was more likely than synaptic scaling to underlie the acetylcholine-induced transition to dispersed firing because of the longer time-scale of activity homeostasis [2]. However, STD was already included in the computational model before this work, and could not reproduce the experimentally observed dispersed firing. This became apparent only after the addition of activity homeostasis, Turrigiano described that activity homeostasis operates over different temporal and spatial timescales [21]. It might be the case that faster-acting mechanisms handle the dynamic switch from burst-dominated network activity to dispersed firing.

4.2 Memory consolidation

It was not possible to induce a second memory trace with low-frequency stimulation in other work, whereas this was possible *in vitro* [2, 18]. Different STDP rules exist that influence, for example, the stability of synapses [19]. It was hypothesized that additive STDP resulted in a stable network state, whereas multiplicative STDP resulted in an unstable network. Other research confirms the hypothesis, that showed that additive STDP is stable, but has difficulties in learning [19]. Multiplicative STDP learns easily but has problems in retention of memory because of instability [19].
We found that implementing activity homeostasis enabled the *in silico* networks to induce a second memory trace. Other work suggested the bi-modal distribution of synaptic weights as the limiting factor for consolidating a second memory trace [18]. However, in current results, this distribution was still present, while networks could consolidate a second trace. This suggests that synaptic plasticity was insufficient for reproducing this experimental finding. Activity homeostasis enhances synaptic plasticity. This is reflected by the extended time needed for the model to find a balance between activity and connectivity (6h vs 2h [18]). It does not imply that activity homeostasis is the only mechanism *in vitro*, but the stability of the synapses is probably an important factor.
It is suggested to investigate other STDP rules for future research, as other work describes that a bi-modal distribution is biologically unlikely [38]. A long-tailed distribution is found to be more likely. STDP rules influence the synaptic weight distribution [19]. Therefore, it will be useful to investigate other rules. In addition, other plasticity mechanisms could be added to the model, but this will introduce more complexity to the model, which is undesired unless proven necessary.

4.3 Prediction

With prediction, the goal of this thesis was to investigate whether neurons can anticipate future events, where events are defined as electrical stimulation. Inter-stimulus intervals from a known distribution were used to investigate prediction. The validation of *in vitro* data showed that the computational model can reproduce results from cortical cultures.

4.3.1 Mutual information

Mutual Information (MI) is used to investigate the prediction of the upcoming stimulation in the computational model. It describes to which extent neuronal activity can reduce the uncertainty on the upcoming stimulation. MI is highest at time-shifts of -100 and 0 ms. These time-shifts corresponds to the bins in which stimulus responses occur. The relation is likely strong because of the recognizable stimulus responses. For positive stim-shifts (activity preceding stimulation), we found maximum prediction 2.0s ahead, coinciding with the most probable ISI value. MI curves show a plateau for time-shifts smaller than the minimum ISI, followed by a peak at the most probable ISI and a subsequent decrease that reflects the distribution of ISIs. It shows that neural activity reduces uncertainty on the next stimulation in this period.
The plateau is caused by the refractory period (i.e. the period in which there cannot be a stimulus). After a stimulus is given, we are sure for the duration of the minimum ISI value that there will be no stimulus. However, the value for MI is still low compared to the values found for [-100, 0] ms. Most bins in the stimulus signal are zero. Therefore, a stimulus (bin with 1) gives MI about future activity, as a stimulus-response is likely. After a stimulus, we are sure that for a certain amount of time we do not have the next stimulus. However, as a bin with a zero is likely, there is only a small reduction in uncertainty. Hence, the relatively small value for MI in this plateau. This hypothesis can be confirmed by increasing the bin size, to improve the ratio of ones to zeros.
We hypothesize that the peak at the time-shift with the most occurring ISI value is caused by a stimulus-response. This hypothesis describes it is most likely that another stimulus-response will occur after an interval with a duration of the most occurring ISI value. However, it is unknown if this is true or if activity between stimulus responses provides information. With post-processing, we randomly set all bins within stimulus responses to zero or one, to make stimulus responses unrecognizable. This randomness caused the decrease of MI and flattening of MI curves, which confirms the hypothesis. Thus, stimulus responses must provide MI.

Limitations

The dependency of the MI on the characteristics of the ISI distribution makes it hard to believe that the results show prediction. In other work, MI rises towards a high value near a time-shift of 0 ms [39]. Their research used MI analysis with visual sensory neurons and stimulated with a stochastic moving bar. Palmer found a maximum MI of 80 ms before a stimulus occurred. We used bins of 100 ms in this research, based on a compromise on precision and computational cost. The bin sizes may have been too large to observe prediction.
We computed MI via a small subset of neurons, to reduce computational cost and the stimuli in the current analysis. Memory is a network effect and believed to be related to prediction [5]. This relation might show that prediction is a network effect as well. We suggest investigating MI between the network activity and the stimuli. Such a method could be applied by assigning values to bins based on the overall activity (i.e. many neurons fired leads to a high value and vice versa). This paradigm limits computational costs and could be used to investigate the MI provided by network activity.

Future directions

For future research, we suggest investigating stimulation patterns with a spatial component, like in other work [39]. A method would be to stimulate individual electrodes in a pattern and add a stochastic component (i.e. unexpected changes in the pattern). Changes in network structure (i.e. synaptic strengths) might be interesting to investigate in prediction. Luczak and colleagues describe that a wrong prediction might cause synaptic changes even without feedback, as this might show unsuccessful learning [40]. If the network changes its structure after an unexpected event, then the anticipation of future states might be proven.
It is suggested to first investigate smaller time bins, as the resolution of the MI analysis might be too low for prediction. If prediction cannot be proven, a change in the experimental design should be made, with some suggestions above.

4.4 Conclusion

Activity homeostasis was not only important for memory consolidation but also enabled the model to reproduce the change from burst dominated network activity to dispersed firing following acetylcholine intervention and reduction of network excitability. We found that activity homeostasis can regulate the firing rate in the computational model. It enhanced synaptic plasticity and enabled the induction of a second memory trace with low-frequency stimulation. A high network excitability may be essential to consolidate memory. With the current analysis, it was not possible to prove prediction. Nonetheless, the model adequately reproduced *in vitro* results and may be used to investigate new stimulation strategies before they are applied *in vitro*.

Bibliography

[1] Antonio Novellino and José-Manuel Zaldívar. Recurrence quantification analysis of spontaneous electrophysiological activity during development: Characterization of in vitro neuronal networks cultured on multi electrode array chips. *Advances in Artificial Intelligence (16877470)*, 2010.

[2] Inês Dias, Marloes R Levers, Martina Lamberti, Gerco C Hassink, Richard van Wezel, and Joost le Feber. Consolidation of memory traces in cultured cortical networks requires low cholinergic tone, synchronized activity and high network excitability. *Journal of Neural Engineering*, 18(4):046051, May 2021.

[3] Dijkstra J. Adaptation to low-frequent stimulu in computational and neuronal networks. *University of Twente*, 2014.

[4] Tanguy Fardet, Mathieu Ballandras, Samuel Bottani, Stéphane Métens, and Pascal Monceau. Understanding the generation of network bursts by adaptive oscillatory neurons. *Frontiers in neuroscience*, 12:41, 2018.

[5] Jeff Hawkins, Dileep George, and Jamie Niemasik. Sequence memory for prediction, inference and behaviour. *Philosophical Transactions of the Royal Society B: Biological Sciences*, 364(1521):1203–1209, May 2009.

[6] Hasker P Davis and Larry R Squire. Protein synthesis and memory: a review. *Psychological bulletin*, 96(3):518, 1984.

[7] Henry L Roediger III, Yadin Ed Dudai, and Susan M Fitzpatrick. *Science of memory: Concepts.* Oxford University Press, 2007.

[8] Steffen Gais and Jan Born. Declarative memory consolidation: mechanisms acting during human sleep. *Learning & Memory*, 11(6):679–685, 2004.

[9] Michael E Hasselmo. The role of acetylcholine in learning and memory. *Current Opinion in Neurobiology*, 16(6):710–715, December 2006.

[10] Mark G. Baxter and Johanna L. Crimins. Acetylcholine receptor stimulation for cognitive enhancement: Better the devil you know? *Neuron*, 98(6):1064 – 1066, 2018.

[11] Marina R. Picciotto, Michael J. Higley, and Yann S. Mineur. Acetylcholine as a neuromodulator: Cholinergic signaling shapes nervous system function and behavior. *Neuron*, 76(1):116–129, October 2012.

[12] Joost Le Feber, Irina I Stoyanova, and Michela Chiappalone. Connectivity, excitability and activity patterns in neuronal networks. *Physical biology*, 11(3):036005, 2014.

[13] Bubic. Prediction, cognition and the brain. *Frontiers in Human Neuroscience*, 2010.

[14] Pau Vilimelis Aceituno, Masud Ehsani, and Jürgen Jost. Spiking time-dependent plasticity leads to efficient coding of predictions. *Biological Cybernetics*, 114(1):43–61, December 2019.

[15] D. Eytan and S. Marom. Dynamics and effective topology underlying synchronization in networks of cortical neurons. *Journal of Neuroscience*, 26(33):8465–8476, August 2006.

[16] Shimon Marom and Goded Shahaf. Development, learning and memory in large random networks of cortical neurons: lessons beyond anatomy. *Quarterly Reviews of Biophysics*, 35(1):63–87, February 2002.

[17] J. le Feber, T. Witteveen, T. M. van Veenendaal, and J. Dijkstra. Repeated stimulation of cultured networks of rat cortical neurons induces parallel memory traces. *Learning & Memory*, 22(12):594–603, November 2015.

[18] T.M. Veenendaal van. Computational modelling of memory in neuronal networks. *Master's thesis*, 2012.

[19] Guy Billings and Mark CW van Rossum. Memory retention and spike-timing-dependent plasticity. *Journal of neurophysiology*, 101(6):2775–2788, 2009.

[20] Gina G. Turrigiano and Sacha B. Nelson. Homeostatic plasticity in the developing nervous system. *Nature Reviews Neuroscience*, 5(2):97–107, February 2004.

[21] Gina G Turrigiano. The self-tuning neuron: synaptic scaling of excitatory synapses. *Cell*, 135(3):422–435, 2008.

[22] David Stellwagen and Robert C Malenka. Synaptic scaling mediated by glial tnf-α. *Nature*, 440(7087):1054–1059, 2006.

[23] EA Neale, WH Oertel, LM Bowers, and VK Weise. Glutamate decarboxylase immunoreactivity and gamma-[3h] aminobutyric acid accumulation within the same neurons in dissociated cell cultures of cerebral cortex. *The Journal of Neuroscience*, 3(2):376–382, February 1983.

[24] Masumi Ichikawa, Kazuyo Muramoto, Kazuo Kobayashi, Masahiro Kawahara, and Yoichiro Kuroda. Formation and maturation of synapses in primary cultures of rat cerebral cortical cells: an electron microscopic study. *Neuroscience Research*, 16(2):95–103, February 1993.

[25] E. M. Izhikevich. Simple model of spiking neurons. *IEEE Transactions on Neural Networks*, 14(6):1569–1572, 2003.

[26] Wickliffe C Abraham, Owen D Jones, and David L Glanzman. Is plasticity of synapses the mechanism of long-term memory storage? *NPJ science of learning*, 4(1):1–10, 2019.

[27] Alain Destexhe, Zachary F Mainen, and Terrence J Sejnowski. Synthesis of models for excitable membranes, synaptic transmission and neuromodulation using a common kinetic formalism. *Journal of computational neuroscience*, 1(3):195–230, 1994.

[28] Sen Song, Kenneth D. Miller, and L. F. Abbott. Competitive hebbian learning through spike-timing-dependent synaptic plasticity. *Nature Neuroscience*, 3(9):919–926, September 2000.

[29] Taro Toyoizumi, Megumi Kaneko, Michael P. Stryker, and Kenneth D. Miller. Modeling the dynamic interaction of hebbian and homeostatic plasticity. *Neuron*, 84(2):497–510, 2014.

[30] Jon Palacios-Filardo and Jack R Mellor. Neuromodulation of hippocampal long-term synaptic plasticity. *Current Opinion in Neurobiology*, 54:37–43, February 2019.

[31] Henry Markram and Misha Tsodyks. Redistribution of synaptic efficacy between neocortical pyramidal neurons. *Nature*, 382(6594):807–810, August 1996.

[32] T. A. Gritsun, J. Le Feber, J. Stegenga, and W. L. C. Rutten. Network bursts in cortical cultures are best simulated using pacemaker neurons and adaptive synapses. *Biological Cybernetics*, 102(4):293–310, February 2010.

[33] Anirudh Gupta, Yun Wang, and Henry Markram. Organizing principles for a diversity of gabaergic interneurons and synapses in the neocortex. *Science*, 287(5451):273–278, 2000.

[34] Henry Markram, Yun Wang, and Misha Tsodyks. Differential signaling via the same axon of neocortical pyramidal neurons. *Proceedings of the National Academy of Sciences*, 95(9):5323–5328, 1998.

[35] Asher Uziel, Henry Markram, et al. t synchrony generation in recurrent networks with frequency-dependent synapses. *Journal of Neuroscience*, 20(1):RC50–RC50, 2000.

[36] Daniel A Wagenaar, Radhika Madhavan, Jerome Pine, and Steve M Potter. Controlling bursting in cortical cultures with closed-loop multi-electrode stimulation. *Journal of Neuroscience*, 25(3):680–688, 2005.

[37] Nicholas M Timme and Christopher Lapish. A tutorial for information theory in neuroscience. *eneuro*, 5(3), 2018.

[38] Jun-nosuke Teramae. Long-tailed distribution of synaptic strength reveals origin and functional roles of ongoing fluctuation in cortical circuit. In *AIP Conference Proceedings*, volume 1738, page 210016. AIP Publishing LLC, 2016.

[39] Stephanie E. Palmer, Olivier Marre, Michael J. Berry, and William Bialek. Predictive information in a sensory population. *Proceedings of the National Academy of Sciences*, 112(22):6908–6913, May 2015.

[40] Artur Luczak, Bruce L. McNaughton, and Yoshimasa Kubo. Neurons learn by predicting future activity. September 2020.